

My chapter

2 Contents

3	1 Spike Train Statistics from Empirical Facts to Theory: The Case of the Retina...	vii
4	Bruno Cessac and Adrian Palacios	
5	1.1 Introduction	vii
6	1.1.1 Chapter Overview	vii
7	1.2 Unraveling the Neural Code in the Retina via Spike Train Statistics Analysis	viii
8	1.2.1 Retina Structure and Functions	viii
9	1.2.2 Multi-Electrodes Array Acquisition	x
10	1.2.3 Encoding a Visual Scene	xii
11	1.2.4 The Ganglion Cells Diversity	xii
12	1.2.5 Population Code	xiii
13	1.3 Spike Train Statistics from a Theoretical Perspective	xiii
14	1.3.1 Spike Statistics	xiii
15	1.3.2 Determining the "Best" Markov Chain to Describe an Experimental Raster	xvii
16	1.4 Using Gibbs Distributions to Analysis Spike Trains Statistics	xxiv
17	1.4.1 Are Ganglion Cells Independent Encoders?	xxv
18	1.4.2 Weak-Pairwise Correlations Imply Strongly Correlated Network States in a	
19	Neural Population.	xxv
20	1.4.3 The Architecture of Functional Interaction Networks in the Retina	xxvi
21	1.4.4 Spike Train Analysis in a Neural Network Model	xxvii
22	1.5 Conclusion	xxx
23	1.5.1 Ising or not Ising?	xxx
24	1.5.2 Linear Potentials versus Combinatorial Explosion	xxxi
25	1.6 Outlook	xxxi
26	1.6.1 Gibbs Distributions and the Neural Code	xxxi
27	1.6.2 Experimental Limits	xxxii
28	1.7 Online Resources	xxxii
29	1.7.1 Database	xxxii
30	1.7.2 Software	xxxiii
31	References	xxxiii
32	References	xxxv
33	Index	xxxvii

Chapter 1

Spike Train Statistics from Empirical Facts to Theory: The Case of the Retina.

Bruno Cessac and Adrian Palacios

Abstract This chapter focuses on methods from statistical physics and probability theory allowing the analysis of spike trains in neural networks. Taking as an example the retina we present recent works attempting to understand how retina ganglion cells encode the information transmitted to the visual cortex via the optical nerve, by analyzing their spike train statistics. We compare the maximal entropy models used in the literature of retina spike train analysis to rigorous results establishing the exact form of spike train statistics in conductance-based Integrate-and-Fire neural networks.

1.1 Introduction

Given a stimulus from the external world (e.g., visual scene, sound or smell) biological sensors at the periphery of the nervous system are able to transduce the physical manifestations of this stimulus (light emission, air pressure variations, chemical concentrations) into sequences of action potentials (spike trains), which propagate through the nervous system. Then, the brain is able to *analyze* those spike trains and infer crucial information on the nature of the stimulus. Critical - yet unsolved - questions in neuroscience are How is the physical signal encoded by the nervous system? How does the brain analyze the spike trains? What are the underlying computational *coding* principles? At the current stage of scientific knowledge, answering those questions is still a challenge for biology and computational neuroscience.

Among sensory systems the retina provides functionality such as detection of movement, orientation, temporal and spatial prediction, response to flash omissions and contrast, that were up to recently viewed as the exclusive duty of higher brain centers [24]. The retina is an accessible part of the brain [15] and a prominent system to study the neurobiology and the underlying computational capacity of the neural coding. As a matter of fact, there is currently a wide research activity in understanding how the retina encodes visual information. However, basic questions are still open, such as: Are the ganglion cells (which send spikes from the eyes to the brain via the optical nerve), independent signal-encoders or are neural correlations important for coding a visual scene, and how to interpret them?

1.1.1 Chapter Overview

Public

This chapter addresses to readers having a master degree in Mathematics, Physics or Biology.

B. Cessac
INRIA Sophia Antipolis Méditerranée, Neuromathcomp project-team, 2004 Route des Lucioles, 06902 Sophia Antipolis Cedex, France, e-mail: bruno.cessac@inria.fr

A. G. Palacios
CINV-Centro Interdisciplinario de Neurociencia de Valparaíso, Universidad de Valparaíso, Harrington 287, Valparaíso 2360102, Chile, e-mail: adrian.palacios@uv.cl

64 Outline

65 In this chapter, we present a state of the art about neural coding in the retina considered from the point
 66 of view of statistical physics and probability theory. As a consequence, this chapter contains both recent
 67 biological results and mathematical developments. The chapter is organized as follows. In Sect. 1.2 we
 68 introduce the current challenge of unraveling the neural code via spike trains statistics analysis. Such an
 69 analysis requires elaborated mathematical tools introduced in Sect. 1.3. We mainly focus on the so-called
 70 Gibbs distributions. This concept come from statistical physics but our presentation departs from the
 71 classical physics courses since it is based on transition probabilities of Markov process. This way, as we
 72 show, allows to handle non-stationary dynamics, and is adapted to statistical analysis, of data as well
 73 as neural networks models. As an illustration, we present, in Sect. 1.4, two "success stories" where spike
 74 train statistics analysis has allowed to make a step further in our understanding of information encoding
 75 by the retina. In the same section, we also present an example of a rigorous spike train analysis in a
 76 neural network and compare the spike trains probability distribution to the models currently used on the
 77 experimental side.

78 1.2 Unraveling the Neural Code in the Retina via Spike Train Statistics 79 Analysis

80 1.2.1 Retina Structure and Functions

81 1.2.1.1 Retina Structure

82 The vertebrate retina is a tightly packed neural tissue, exhibiting a rich diversity of neurons. It is struc-
 83 tured in three cells nuclei layers and two plexiform synaptic layers [37, 77] (Fig. 1.1(a)). The outer nuclear
 84 layer (ONL) contains the rods and cones *photoreceptors* (P) somata; the inner nuclear layer (INL) contains
 85 *bipolar* (B), *horizontal* (H) and *amacrine cells* (A). Finally, the most internal nuclear layer is composed
 86 with ganglion cells (G) and displaced amacrine cells. The outer plexiform layer (OPL) corresponds to synaptic
 87 contacts between P, B and H cells. The inner plexiform layer (IPL) corresponds to synaptic
 88 contacts between B, A and G cells.

89 The retina is about $300 - 500\mu m$ thick, depending on species, and has about $100 - 130$ millions of
 90 photoreceptors, $10 - 12$ millions of bipolar, horizontal and amacrine cells and 0.4 to 1.6 millions of G cells.
 91 Together with this high and compact number of cells there is a very large number of synapses present in
 92 dendrites and axons terminal, that has been roughly estimated to 1 billion of synapses [58]. The retina
 93 is also rich in terms of the variability of neurotransmitters, where rods, cones, and bipolar cells liberate
 94 glutamate, horizontal and amacrine cells can liberate gaba, glycine, serotonin, acetylcholine, dopamine
 95 among others. Together with the richness in chemical slow synapses circuits the retina has a variety of
 96 electrical ("gap-junctions"), fast synapses endowing the retina with specific functional circuits.

97 Single photons are converted by photoreceptors into a graded change in the resting potential, resulting
 98 in a neurotransmitter liberation (glutamate) into the synaptic region connecting photoreceptors with B
 99 and H cells. Those cells make synapses with G and A cells. Therefore, photons fluxes generate a chain of
 100 changes in the resting potential of B,H,A, and G cells with consequence the emission of action potentials
 101 ("spikes") by G cells. They are the principal neural encoders through the integration of neural signals.
 102 The retina output, formed by spike train sequence, is carried by different types of G cells through the
 103 optical nerve to the brain higher visual structures: *e.g.* lateral geniculate nucleus (LGN) or visual cortex
 104 layers (Fig. 1.2).

106 1.2.1.2 Retina Circuits and Receptive Fields

107 As a result of its stratified, horizontal and vertical structure, and of the various type of synaptic con-
 108 nections (electrical fast synapses $\sim 0.1 ms$ for short distance; chemical slow synapses $\sim 10 ms$ for long
 109 distances) between the different type of neurons (P,H,B,A,G) a large number of "circuits" are present in

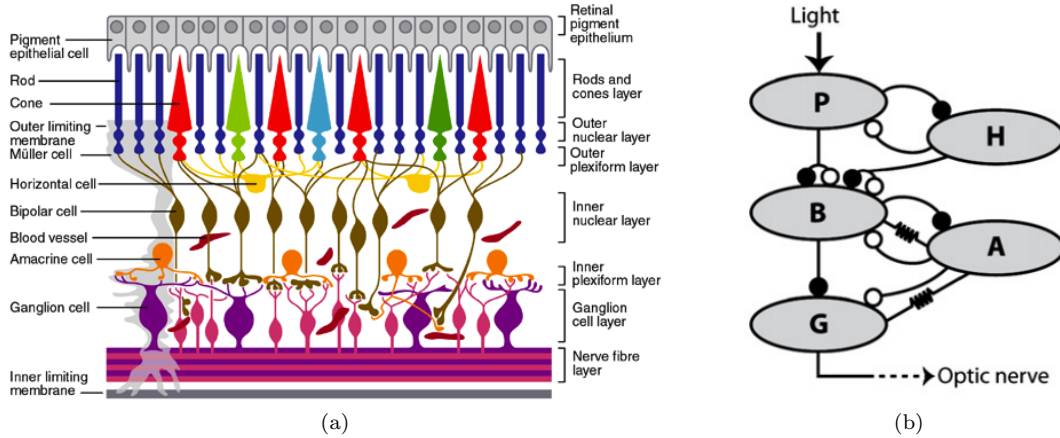
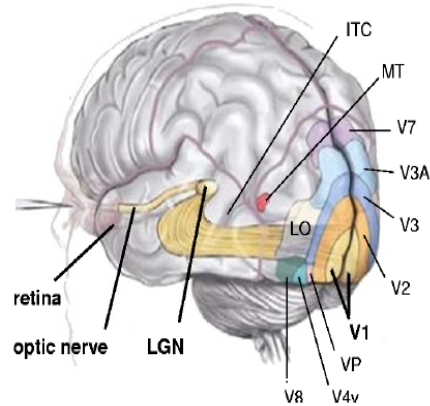


Fig. 1.1 Processing steps of the visual stream. (a) The cellular organization of the retina (from Expert Reviews in Molecular Medicine by Cambridge University Press 2004); (b) Main connectivity structure between retina cells types (from [24])

Fig. 1.2 Visual Pathway in the human brain. The principal projection of the eye, which is formed by the optic nerve is carried to a first synapses in the lateral geniculate nucleus (LGN) in the thalamus and then for a second synapses to the main cortical visual area V1, from where many other projections target secondary cortical areas (V2, etc). Reproduced from [32].



110 the retina. The main connectivity structure of the retina is shown in Fig. 1.1(b). This circuitry results in
 111 the capacity of specific G cells to respond to specific stimuli in the visual field.

112 The *receptive field* (RF) of a sensory neuron is a region of space where the presence of a stimulus
 113 modifies the activity of that neuron. In the retina this change of activity is precisely the result of the
 114 transduction chain, from photoreceptor to G cells, converting photons into spike trains. As a consequence,
 115 one also defines the RF of a G cell as the input from all of the photoreceptors which synapse with it (via
 116 B, H, A) cells.

117 The RF of a cell can have different forms, depending on the network of neurons connected to this cell.
 118 A prominent example, is the *antagonist ON-OFF center-surround arrangement*. First, photoreceptors
 119 make synapses with ON (excitatory) B cells and OFF (inhibitory) B cells according to their response to
 120 light. The physiological properties of G cells are determined at the center and the surround of their RF
 121 by the input of ON or OFF B cell.

122 Fig. 1.3(a) explains in a schematic way how this property results from the connectivity between P, B,
 123 and H cells. In the example, the illumination of the photoreceptors in the center of the RF results in a
 124 depolarization of ON B cells so in an increase of spikes rate in the respective connected G cells. On the
 125 opposite, the illumination of the photoreceptors at the periphery of the RF results in a hyper-polarization
 126 of OFF B cells so in a decrease of spikes rate in the respective connected G cells. In more general terms,
 127 as a consequence of this architecture (Fig. 1.3(a)), a G cell connected to that B cell fires spikes at the
 128 maximal rate when the center of the RF is illuminated and when the surround is dark (Fig. 1.3(b-2),
 129 case 3). On the opposite it fires no spike at all when the center of the RF is dark and the surround is
 130 illuminated (Fig. 1.3(b-4) case 4).

131 Fig. 1.3(b) summarizes the different patterns of illuminations - G cell response in terms of spike firing
 132 and the functional implication of RF organization. For example, a full, uniform, illumination of the RF

133 leads to a regular spiking activity with no difference between ON-OFF and OFF-ON cells (Fig. 1.3(b),
 134 case 5).

135 As consequence of dynamical and complex interaction (spatial and temporal) opposite functions for,
 136 *e.g.*, color, contrast, intensity are likewise found for a single G cell, depending where the stimulus is
 137 present in their RF.

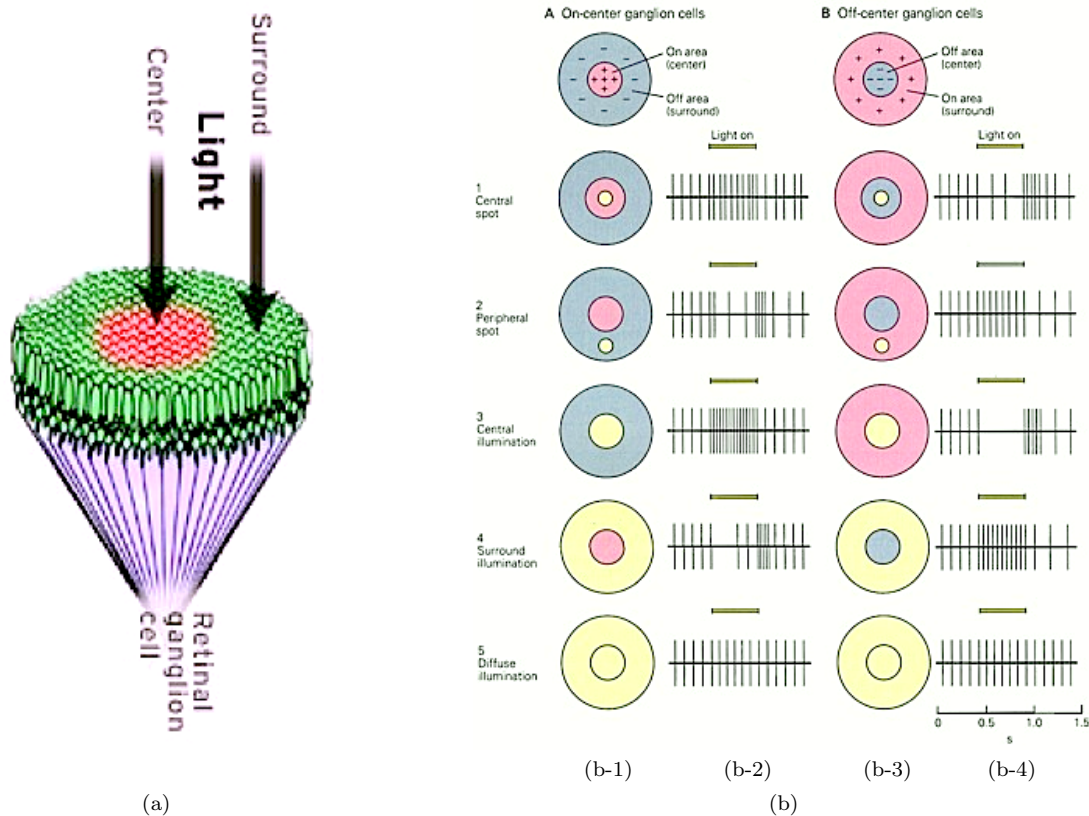


Fig. 1.3 Center-Surround antagonism (a) Illumination of a piece of retina (from <http://www.webexhibits.org/colorart/ganglion.html>). (b) ON-center and OFF-center RF, Figure from [1]. The first line shows center-surround architecture of the cell while lines 2-6 shows a typical response of the G cells and the illumination pattern leading to that response. (b-1) Center-surround architecture of an ON-center cell and illumination pattern. (b-2) Time duration of the stimulus and spike response of the cell. Time is in abscissa. (b-3) and (b-4) Same as columns (b-1) and (b-2) for an OFF-center cell. Case 1 left (right) is a ON-center (OFF-center) G cell where a light spot (yellow) in the center of the RF generates an increase (decrease) of spike firing. In case 2 a spot stimulus in the surround generates a decrease (increase) of the spike rate. In case 3,4 an increase in the size of the stimuli leads a sharper response. In case 5 a diffuse stimulus covering the center-periphery has no effect on the spike firing rate.

138 It has been long believed that retina was mainly acting as an image transducer, absorbing photons
 139 and producing electrical signals or acting as a temporal and spatial linear filter. It was also believed that
 140 the retina doesn't perform any pre-processing of the image before sending spike trains to the brain. More
 141 recently, researchers pointed out that retina, in some species, is "smarter" than previously believed and
 142 is able to detect salient features or properties in a image such as approaching motion, motion detection
 143 and discrimination, texture and object motion, creating predictive or anticipatory coding thanks to
 144 "specialized" G cells (see, *e.g.*, [24] for a review). The specificity of these population of cells for the
 145 detection of differential motion results largely from the circuit they belong to. An example is shown in
 146 Fig. 1.4 (detection of differential motion) where A cells play a prominent role.

147 1.2.2 Multi-Electrodes Array Acquisition

148 The pioneering work of Hubel and Wiesel based on anatomy and single cell recording on brain vi-
 149 sual areas was very useful. However at that time, little was known about the properties of the reti-

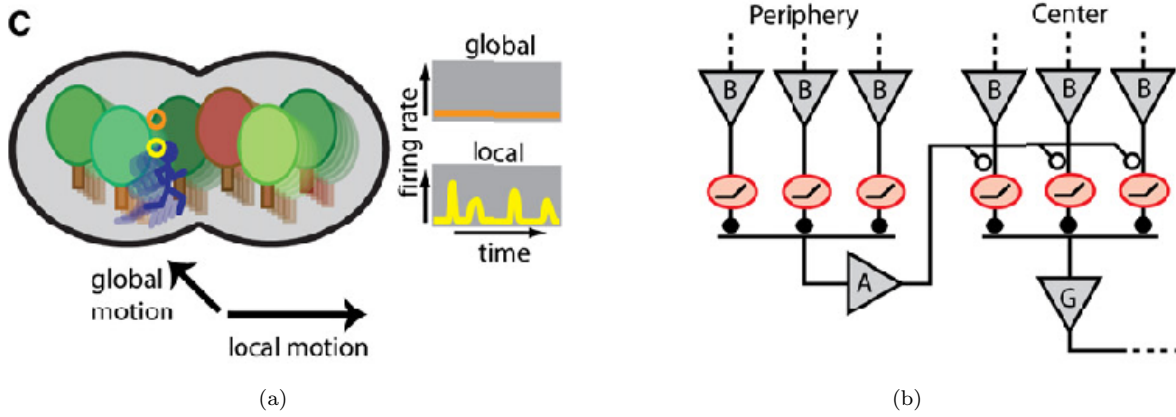


Fig. 1.4 Detection of differential motion. (a) An object-motion-sensitive G cell remains silent under global motion of the entire image but fires when the image patch in its RF moves differently from the background. (b) Scheme summarizing the circuitry behind this computation. Rectification (see [13] for a description of rectification mechanism.) of B cell signals in the RF center creates sensitivity to motion. Polyaxonal A cells in the periphery are excited by the same motion-sensitive circuit and send inhibitory inputs to the center. If motion in the periphery is synchronous with that in the center, the excitatory transients will coincide with the inhibitory ones, and firing is suppressed (Fig. from [24]. The legend is adapted from this reference).

150 nal neural network. Similarly, today, the anatomical description of different types of G cells is a well
 151 known piece of literature, in contrast to their collective neural response that is partly missing. To
 152 overcome limitations of single-electrodes recording and to access to the coding response of a popula-
 153 tion of neurons, multi-electrodes (MEA) devices are used in physiology (for references on MEA see
 154 [69]). MEA devices are formed by an array of isolated electrodes (64 to 256, separated from 30- 200
 microns each, see Fig. 1.5). When in contact with a small piece of neural tissue, a MEA is able to

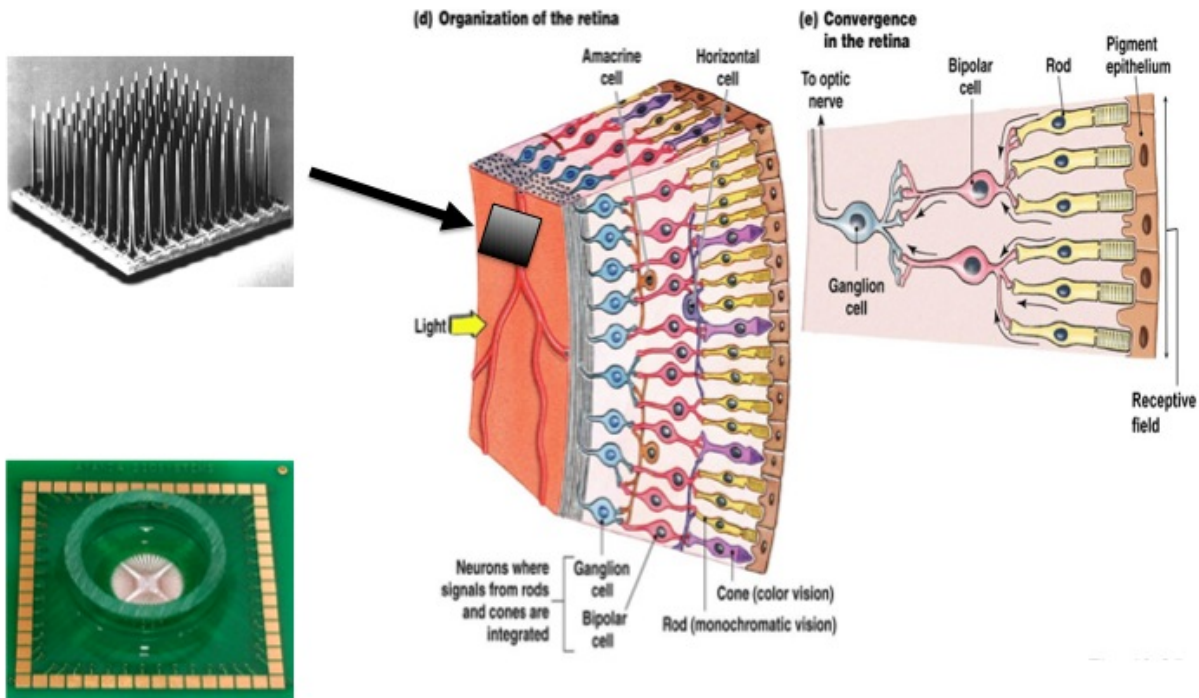


Fig. 1.5 Left: Up: "Utah MEA" from <http://www.sci.utah.edu/>. Down: Multi Electrode Array Bioship from <http://t3.gstatic.com/>. Right: Schematic view of the implantation of a MEA on the retina.

155 record the simultaneous activity (spike and/or field potential) from, e.g., 10-150 G cells. The final goal
 156 is to produce from the MEA signal a *raster plot* of G cells activity, namely a graph with time in ab-
 157

158 scissa and a neuron labeling in ordinate such that a vertical bar is drawn each "time" a neuron emits
 159 a spike. This poses an important challenge for signal processing: to sort out from a complex (spatial
 160 and temporal) neural signal superposition recording the contribution of each cell. With the recent in-
 161 crease in the number of electrodes of MEA devices, the necessity of adequate spike sorting algorithms
 162 turns out to be critical. Recently the Berry's lab at Princeton has developed an efficient method, en-
 163 abling to sort out, from a 256 MEA experiment, about 200 different G cells (personal communication).

164
 165 MEA devices constitute an excellent tool to track the physiological properties of G cells [45] as well
 166 as their coding capacity [29, 30]. Before the introduction of MEA devices, the neural coding properties of
 167 single G cells was study using intra or extra cellular electrodes, giving a limited sense of their collective
 168 role. In that respect, the work of Markus Meister *et al.* [40] using MEA devices was pioneer. With simple
 169 stimulus, like checkerboard random white noise, and spike sorting algorithms these authors were able to
 170 determinate the number of spiking cells and their respective RF. They have shown that concerted G cells
 171 are critical, not only for retina development, but for the neural coding processing.

172 *1.2.3 Encoding a Visual Scene*

173 The distribution and fluctuations of visual signals in the environment can be treated as a statistical
 174 problem [43, 67]. Natural scenes (a digital image or movie from a natural scenario) differ in their particular
 175 statistical structure and therefore the encoding capacity of a visual system should be able to match the
 176 properties and distribution of visual signals in the environment where the organism lives [3, 20, 21, 70, 72].
 177 The anatomical and physiological segregation of different aspects of a visual scene in separate spatial,
 178 temporal and chromatic channels start at the retina and rely on local "circuits" [3]. However, how the
 179 precise articulation of this neural network contributes to local solutions and global perception is still
 180 largely a mystery.

181 G cells, as well as most neurons in the nervous system respond to excitations, coming from other neu-
 182 rons or from external stimuli, by emitting spike trains. In the contemporary view [48], spikes are quantum
 183 or bits of information and their spatial (neuron-dependent) and temporal (spike times) structure carry
 184 "information": This is called "the" "neural code". Although this view is strongly based on a contem-
 185 porary analogy with computers, spike trains *are not* computer-like binary codes. Indeed, an experiment
 186 reproduced several times (*e.g.*, an image presented several times to the retina) does not reproduce ex-
 187 actly the same spike train, although some regularity is observed. As a consequence, current attempts to
 188 deciphering the neural code are based on statistical models.

189 *1.2.4 The Ganglion Cells Diversity*

190 The recent use of MEA in retina has lead to the description of a diversity of G cells type and to the question
 191 about their actual early visual capacity. The vertebrate retina has in fact 15-22 anatomically different
 192 class of G cells making it a much more complex functional neural network than expected [37, 49, 24].

193 The three most frequent G cells in the retina can be classified from their morphology in: parasol
 194 (primates but α or Y in cats and rabbits) corresponding to 3-8% of the total number of G cells; midget
 195 (β or X in cats and rabbits) corresponding to 45-70%; and bi-stratified G cells. In physiological terms
 196 parasol (Y) cells can be classified as brisk-transient, and midget (X) as brisk-sustained. They can have
 197 an ON or OFF function.

198 Although only a reduced fraction of the existing G cells [37, 38, 62] has been studied in detail [24],
 199 their diversity raises questions such as: How do G cells encode an image? Which features from a natural
 200 visual scene are they coding? Are G cells independent or collective encoders?

An interesting approach has been advanced by [5]. The authors propose that the retina organization
 should use simple coding principles to carry the maximum of information at low energetic cost. However,
 as the authors point out, the statistic distribution (*e.g.*, color, contrast) for natural images is *not* Gaussian.
 Therefore, the classical Gaussian estimator for Shannon information:

$$I = \frac{1}{2} \log_2 (1 + SNR),$$

201 where SNR is the signal to noise ratio is not appropriate. Instead, "pixels" in natural images are highly
 202 correlated and the general form of statistical entropy (see Eq. (2) in [5]) is required to calculate the spike
 203 capacity of G cells to carry information. In that respect, the coding capacity for different G cells has been
 204 estimated (see, *e.g.*, Eq. (5) in [5]). The larger capacity for information transmission comes from, *e.g.*,
 205 "sluggish" G cells (32%); local-edge (16%), brisk-transient (9%).

206 **1.2.5 Population Code**

207 This term refers to the computational capacity of a neural assembly (or circuit) to solve specific questions
 208 [4, 47]. Assuming that living systems have evolved to optimize the population code, how is this optimum
 209 reached in the retina? Are G cells sensors independent encoders or, on the opposite, are neural correlations
 210 important for coding? In an influential article, Nirenberg *et al.* [41] suggest that G cells act as independent
 211 encoder. However, orchestrated spikes train from G cells were reported by pioneer work of Rodieck [50]
 212 and Mastronarde [39]. Mastronarde shows that G cells responses tend to fire together and dynamically
 213 adapt to light or dark background [39]. This suggests that they act in a correlated way. However, this
 214 approach is by itself incomplete, since different sources of correlation were not clearly considered [44, 61].
 215 On the other hand, MEA can now record many G cells from small pieces of retina ($< 500\mu m$) [14, 40, 17]
 216 and help us to asses the importance, and origin, of neural synchrony for the neural coding. For example,
 217 in darkness, salamander G cells shows 3 types of synchrony depending on the time laps: (i) a common
 218 photoreceptor source through B cells (*broadcorrelation* : 40 – 100ms) (ii) A cells and G cells connected
 219 through gap junctions (*medium* : 10 – 50ms) (iii) gap junction between G cells (*narrow* : $< 1ms$) [6].

220 At present and although a large bunch of experimental facts enlighten our knowledge about the retina
 221 structure as well as its activity, basic questions on the way how a visual scene is encoded by spike trains
 222 remain still open. This is largely due to (i) the complex structure of the retina; (ii) its large number
 223 of cells; (iii) the lack of sufficiently accurate statistical models and methods to discriminate competing
 224 hypotheses. Apparently elementary questions such as determining whether correlations are significant
 225 from the analysis of MEA recordings requires in fact the use of smart statistical analysis techniques,
 226 based on "statistical models" defined by a set of a priori hypothesis as we see in the next section.

227 **1.3 Spike Train Statistics from a Theoretical Perspective**

228 In this section we develop the mathematical framework to analyze spike train statistics. The collective
 229 neuron dynamics, which is generally submitted to noise, produces spike trains with randomness though
 230 some statistical regularity can be observed. Spike trains statistics is assumed to be summarized by an
 231 hidden probability μ characterizing the probability of spiking patterns. One current goal in experimental
 232 analysis of spike trains is to approximate μ from data. We describe here several theoretical tools allow-
 233 ing to handle this question. Our presentation is based on the notion of transition probabilities. In this
 234 context we introduce Gibbs distributions, which is one of the main theoretical concept of this chapter.
 235 Gibbs distributions are usually considered in the stationary case where they are obtained from the max-
 236 imal entropy principle. Their definition via transition probabilities, adopted in this chapter, affords the
 237 consideration of Gibbs distribution in the more general context of non-stationary dynamics with possibly
 238 infinite memory.

239 **1.3.1 Spike Statistics**

240 **1.3.1.1 Raster Plots**

We consider a network of N neurons. We assume that there is a minimal time scale $\delta > 0$ corresponding
 to the minimal resolution of the spike time, constrained by biophysics and by measurements methods
 (typically $\delta \sim 1ms$) [9, 8]. Without loss of generality (change of time units) we set $\delta = 1$, so that
 spikes are recorded at integer times. One then associates to each neuron k and each integer time n a
 variable $\omega_k(n) = 1$ if neuron k fires at time n and $\omega_k(n) = 0$ otherwise. A *spiking pattern* is a vector

$\omega(n) \stackrel{\text{def}}{=} [\omega_k(n)]_{k=1}^N$ which tells us which neurons are firing at time n . We note $\mathcal{A} = \{0, 1\}^N$ the set of spiking patterns. A *spike block* is a finite ordered list of spiking patterns, written:

$$\omega_{n_1}^{n_2} = \{\omega(n)\}_{\{n_1 \leq n \leq n_2\}},$$

241 where spike times have been prescribed between the times n_1 to n_2 (*i.e.*, $n_2 - n_1 + 1$ time steps). The
 242 *depth* of the block is the number of time steps where time has been prescribed (in the example this is
 243 $n_2 - n_1 + 1$). The set of such blocks is $\mathcal{A}^{n_2 - n_1 + 1}$. Thus, there are 2^{Nn} possible blocks with N neurons
 244 and depth n . For example, $N = 3$ neurons and $n = 2$ time steps the possible blocks are:

$$\begin{pmatrix} 0 & 0 \\ 0 & 0 \\ 0 & 0 \end{pmatrix}; \begin{pmatrix} 0 & 1 \\ 0 & 0 \\ 0 & 0 \end{pmatrix}; \begin{pmatrix} 1 & 0 \\ 0 & 0 \\ 0 & 0 \end{pmatrix}; \begin{pmatrix} 1 & 1 \\ 0 & 0 \\ 0 & 0 \end{pmatrix}; \dots \begin{pmatrix} 1 & 1 \\ 1 & 1 \\ 1 & 0 \end{pmatrix}; \begin{pmatrix} 1 & 1 \\ 1 & 1 \\ 1 & 1 \end{pmatrix}.$$

245 We call a *raster plot* a bi-infinite sequence $\omega \stackrel{\text{def}}{=} \{\omega(n)\}_{n=-\infty}^{+\infty}$, of spiking patterns. This notion corresponds
 246 to its biological counterpart (Sect. 1.2.2) with the obvious difference that experimental raster plots are
 247 finite. The consideration of infinite sequences is more convenient on the mathematical side but, at several
 248 places, we discuss the effects of having finite experimental rasters on spike statistics estimation. The set
 249 of raster plots is denoted $\mathcal{X} = \mathcal{A}^{\mathbb{Z}}$.

250 1.3.1.2 Transition Probabilities

251 The probability that a neuron emits a spike at some time n depends on the history of the neural network.
 252 However, it is impossible to know explicitly its form in the general case since it depends on the past
 253 evolution of all variables determining the neural network state. A possible simplification is to consider
 254 that this probability depends *only* on the spikes emitted in the past by the network. In this way, we are
 255 seeking a family of transition probabilities of the form $P[\omega(n) | \omega_{n-D}^{n-1}]$, the probability that the firing
 256 pattern $\omega(n)$ occurs at time n , given a past spiking sequence ω_{n-D}^{n-1} . Here D is the *memory depth* of the
 257 probability, *i.e.*, how far in the past does the transition probability depend on the past spike sequence.
 258 We use here the convention that $P[\omega(n) | \omega_{n-D}^{n-1}] = P[\omega(n)]$ if $D = 0$ (memory-less case).

259 Transition probabilities depend on the neural network characteristics such as neurons conductances,
 260 synaptic responses or external currents. They give information on the dynamics that takes place in the
 261 observed neural networks. Especially, they have a *causal* structure where the probability of an event
 262 depends on the past. This reflects underlying biophysical mechanisms in the neural networks which are
 263 also causal. The explicit computation of transition probabilities can be done in some model-examples
 264 (Sect. 1.4.4). From them, one is able to characterize statistical properties of rasters generated by the
 265 network, as we now develop.

266 1.3.1.3 Markov Chains

267 Transition probabilities with a finite memory depth D define a “Markov chain”, *i.e.*, a random process
 268 where the probability to be in some state at time n (here a spiking pattern $\omega(n)$) depends only upon a
 269 finite past (here on $\omega(n-1), \dots, \omega(n-D)$). Markov chains have the following property. Assume that we
 270 know the probability of occurrence of the block ω_m^{m+D-1} ,

$$P[\omega_m^{m+D-1}] = P[\omega(m+D-1), \omega(m+D-2), \dots, \omega(m)]. \quad (1.1)$$

Note that, mathematically, the order of the spiking patterns does not matter in the right-hand side since we are dealing with a joint probability, but choosing this specific order is useful for subsequent explanations. Then, by definition, the probability of the block ω_m^{m+D} is:

$$\begin{aligned} P[\omega_m^{m+D}] &= P[\omega(m+D), \omega(m+D-1), \dots, \omega(m)] \\ &= P[\omega(m+D) | \omega(m+D-1), \dots, \omega(m)] P[\omega(m+D-1), \dots, \omega(m)]. \end{aligned}$$

Thus:

$$P[\omega_m^{m+D}] = P[\omega(m+D) | \omega_m^{m+D-1}] P[\omega_m^{m+D-1}],$$

and, by induction, the probability of a block ω_m^n , $\forall n, n - m \geq D$ is given by:

$$P[\omega_m^n] = \prod_{l=m+D}^n P[\omega(l) | \omega_{l-D}^{l-1}] P[\omega_m^{m+D-1}]. \quad (1.2)$$

Thus, knowing the probability of occurrence of the block ω_m^{m+D-1} one can infer the probability of forthcoming blocks by the mere multiplication of transition probabilities.

Given the (joint) probability $P[\omega_m^n]$ the (marginal) probability of sub-blocks can be easily obtained, since for $m \leq n_1 \leq n_2 \leq n$,

$$P[\omega_{n_1}^{n_2}] = \sum_{m,n}^{*(n_1, n_2)} P[\omega_m^n], \quad (1.3)$$

where $\sum_{m,n}^{*(n_1, n_2)}$ means that we sum up over all possible spiking patterns in the interval $\{m, n\}$ excluding the interval $\{n_1, n_2\}$ (*i.e.*, we sum up over all possible values of $\omega(n), \dots, \omega(n_1 - 1), \omega(n_2 + 1), \dots, \omega(n)$).

As a consequence, from (1.2), (1.3), the probability of the spike block ω_{n-D}^n , of depth D , is:

$$P[\omega_{n-D}^n] = \sum_{m,n}^{*(n-D, n)} \prod_{l=m+D}^n P[\omega(l) | \omega_{l-D}^{l-1}] P[\omega_m^{m+D-1}]. \quad (1.4)$$

Knowing the probability of an initial block of depth D (here ω_m^{m+D-1}) one infers from this equation the probability of subsequent blocks of depth D . Equation (1.4) can also be expressed in terms of vector-matrices multiplication, and the main properties of the Markov chain can be deduced from linear algebra and matrices spectra theorems [64]. For compactness we shall not use this possibility here though, (see [75] for further details).

However, this equation shows that the "future" of the Markov chain (the probability of occurrence of blocks) depends on an initial condition (here $P[\omega_m^{m+D-1}]$), which is a priori undetermined. Moreover, there are *a priori* infinitely many possible choices for the initial probability.

1.3.1.4 Asymptotic of the Markov Chain

Assume now that $n - m \rightarrow +\infty$ in Eq. (1.4) and more precisely that $m \rightarrow -\infty$. Practically, this limit corresponds to considering that the system began to exist in a distant past (defined by the initial condition of the Markov chain) and that it has evolved long enough, *i.e.*, over a time larger than relaxation times in the system, so that it has reached sort of an "adult" age where its structure is essentially fixed. Note that this does not exclude adaptation processes, *e.g.*, if the transition probabilities depend explicitly on time. Mathematically, the limit $n - m \rightarrow +\infty$ corresponds to studying the asymptotic of the Markov chain and related questions are: Is there a limit probability $P[\omega_{n-D}^n]$? Does it depend on the initial condition $P[\omega_m^{m+D-1}]$, $m \rightarrow -\infty$?

Let us first consider the easiest case where transition probabilities are invariant under time translation. This means that for each possible spiking pattern $\alpha \in \mathcal{A}$, for all possible "memory" blocks $\alpha_{-D}^{-1} \in \mathcal{A}^D$ and $\forall n$, $P[\omega(n) = \alpha | \omega_{n-D}^{n-1} = \alpha_{-D}^{-1}] = P[\omega(0) = \alpha | \omega_{-D}^{-1} = \alpha_{-D}^{-1}]$. We call this property *stationarity* referring rather to the physics literature than to the Markov chains literature (where this property is called *homogeneity*). If, additionally, all transition probabilities are strictly positive then there is a unique probability μ , called the *asymptotic probability of the chain*, such that, whatever the initial choice of a probability $P[\omega_m^{m+D-1}]$ in (1.4) the probability of a block ω_{n-D}^n converges to $\mu[\omega_{n-D}^n]$ as m tends to $-\infty$. One says that the chain is *ergodic* (Note that positivity of all transition probabilities is a sufficient but not necessary condition for ergodicity [64]). In this sense, dynamics somewhat "selects" the probability μ , since, whatever the initial condition $P[\omega_m^{m+D-1}]$, it provides the statistics of spikes observed after a sufficiently long time. Additionally, μ has the following property: for any time $n_1, n_2, n_2 - n_1 \geq D$,

$$\mu[\omega_{n_1}^{n_2}] = \prod_{l=n_1+D}^{n_2} P[\omega(l) | \omega_{l-D}^{l-1}] \mu[\omega_{n_1}^{n_1+D-1}]. \quad (1.5)$$

Let us return to the problem of choosing the initial probability in Eq. (1.4). If one wants to determine the evolution of the Markov chain after a initial observation time n_1 one has to fix the initial probability $P[\omega_{n_1}^{n_1+D-1}]$ and to use (1.4) (where m is replaced by n_1) and there is an indeterminacy in the choice of $P[\omega_{n_1}^{n_1+D-1}]$. This indeterminacy is released, though, if the system has started to exist in the infinite past. Then, $P[\omega_{n_1}^{n_1+D-1}]$ has to be replaced by $\mu[\omega_{n_1}^{n_1+D-1}]$ and Eq. (1.4) becomes:

$$\mu[\omega_{n_2-D}^{n_2}] = \sum_{n_1, n_2}^{*(n_2-D, n_2)} \prod_{l=n_1+D}^{n_2} P[\omega(l) | \omega_{l-D}^{l-1}] \mu[\omega_{n_1}^{n_1+D-1}]. \quad (1.6)$$

In this way, taking the limit $m \rightarrow -\infty$ for an ergodic Markov chain, resolves the indeterminacy in the initial condition.

Positivity and stationary assumptions may not hold. If positivity is violated then several situations can arise: several asymptotic probability distributions, can exist, depending on the choice of the initial probability $P[\omega_m^{m+D-1}]$; it can also be that no asymptotic probability exist at all. If stationarity does not hold, as it is the case *e.g.* for a neural network with a time-dependent stimulus, then one can nevertheless define a probability μ selected by dynamics. In short, this is a probability μ on the set of raster plots $\mathcal{A}^{\mathbb{Z}}$ which still obeys (1.5) but without the conditions of stationarity (transition probabilities are not time-translation invariant [16]). In this case, which is realistic when dealing with living systems submitted, *e.g.*, to time-dependent stimuli, the statistics of spikes is time-dependent. For example, the probability that a neuron emits a spike at time n depends on n , while it is not the case when dynamics is stationary.

1.3.1.5 Gibbs Distributions

Assume that $P[\omega(n) | \omega_{n-D}^{n-1}] > 0$ for all $n \in \mathbb{Z}$. Then, a probability distribution μ that obeys (1.5) is called a *Gibbs distribution*, and the function

$$\phi_n(\omega_{n-D}^n) \stackrel{\text{def}}{=} \log P[\omega(n) | \omega_{n-D}^{n-1}], \quad (1.7)$$

is called a (normalized) *Gibbs potential*. The advantage of this definition of Gibbs distribution is that it holds for time-dependent transition probabilities contrarily to the classical definition from the maximal entropy principle (Sect. 1.3.2.8). Moreover, in the case (1.7) the Gibbs potential depends explicitly on time (index n). This definition also extends to system with infinite memory (Sect. 1.4.4) although Eq. (1.5) has to be modified [16].

The Gibbs potential depends on the block ω_{n-D}^{n-1} and on the spiking pattern $\omega(n)$, thus, finally, this is a function of the block ω_{n-D}^n of depth $D+1$. The term "normalized" refers to the fact that the potential in (1.7) is the logarithm of a transition probability. Below, we give example of Gibbs distributions where the potential is not normalized: this is an arbitrary function of the block ω_{n-D}^n . We call $R = D+1$ the *range* of the potential. A Gibbs potential can have an infinite range ($D \rightarrow -\infty$ in our setting).

The condition $P[\omega(n) | \omega_{n-D}^{n-1}] > 0$ for all $n \in \mathbb{Z}$ ensures that there is a one-to-one correspondence between a Gibbs potential and a Gibbs distribution. If this condition is relaxed, *i.e.*, some transitions are forbidden, then several Gibbs distribution can be associated with a Gibbs potential. This corresponds to a first-order phase transition in statistical physics [22]. In the infinite range case, the existence and uniqueness of a Gibbs distribution associated with this potential requires additional assumptions to the positivity of transition probabilities [16].

From (1.2), we have $\forall n - m \geq D$:

$$\mu[\omega_m^n | \omega_m^{m+D-1}] = \exp \sum_{l=m+D}^n \phi_l(l, \omega). \quad (1.8)$$

This form reminds the Gibbs distribution on spin lattices in statistical physics where one looks for lattice translation-invariant probability distributions given specific boundary conditions. Given a potential of range D the probability of a spin block depends on the states of spins in a neighborhood of size D of that block. Thus, the conditional probability of this block given a fixed neighborhood is the exponential of the energy characterizing physical interactions within the block as well as with the boundaries. Here, spins are replaced by spiking patterns; space is replaced with time which is mono-dimensional and oriented: there is no dependence in the future. Boundary conditions are replaced by the dependence in the past.

1.3.2 Determining the "Best" Markov Chain to Describe an Experimental Raster

We now show how the formalism of the previous section can be used to analyze spike trains statistics in experimental rasters.

1.3.2.1 Observables

We call *observable* a function which associates to a raster plot a real number. Typical examples are $f(\omega) = \omega_k(n)$ which is equal to '1' neuron k spikes at time n in the raster ω and is '0' otherwise; likewise the function $f(\omega) = \omega_k(n)\omega_{k'}(n)$ is '1' if and only if neuron k and k' fire synchronously at time n in the raster ω . These two cases are example of what we call *monomials* in the chapter, namely functions of the form $\omega_{k_1}(n_1)\omega_{k_2}(n_2)\dots\omega_{k_m}(n_m)$ which is equal to 1 if and only if neuron k_1 fires at time n_1, \dots , neuron k_m fires at time n_m in the raster ω . Thus monomials attribute the value '1' to characteristic spike events. One can also consider more general forms of observables, *e.g.* non linear functions of spike events (see for example Eq. (1.37), (1.41) below).

1.3.2.2 Probabilities and Averages

Let μ be a probability on the set of rasters (typically the Gibbs distribution introduced above). Mathematically, the knowledge of μ is equivalent to knowing the probability $\mu[\omega_m^n]$ of any possible spike block. For an observable f we denote $\mu[f] \stackrel{\text{def}}{=} \int f d\mu$ the average of f with respect to μ . If f is only a function of finite blocks ω_m^n then:

$$\mu[f] = \sum_{\omega_m^n} f(\omega_m^n) \mu[\omega_m^n], \quad (1.9)$$

where the sum holds on all possible (2^{n-m+1}) values of ω_m^n . For example the average value of $f(\omega) = \omega_k(n)$ is given by $\mu[\omega_k(n)] = \sum_{\omega_k(n)} \omega_k(n) \mu[\omega_k(n)]$ where the sum holds on all possible values of $\omega_k(n)$ (0 or 1). Thus, finally

$$\mu[\omega_k(n)] = \mu[\omega_k(n) = 1], \quad (1.10)$$

which is the probability of firing of neuron k at time n . This quantity is called the *instantaneous firing rate*. Likewise, the average value of $\omega_{k_1}(n)\omega_{k_2}(n)$ is the probability that neuron k_1 and k_2 fire at the same time n : this is a measure of *pairwise synchronization* at time n .

1.3.2.3 Empirical Averages

In experiments, raster plots have a finite duration T and one has only access to a finite number \mathcal{N} of those rasters, denoted $\omega^{(1)}, \dots, \omega^{(\mathcal{N})}$. From these data one computes empirical averages of observables. Depending on the hypotheses made on the underlying system there are several ways of computing those averages.

A classical (though questionable assumption as far as experiments are concerned) is *stationarity*: the statistics of spike is time-translation invariant. In this case the *empirical average* reduces to a *time average*. We denote $\pi_\omega^{(T)}[f]$ the time average of the function f computed for the raster ω of T . For example, when $f(\omega) = \omega_k(n)$, $\pi_\omega^{(T)}[f] = \frac{1}{T} \sum_{n=0}^{T-1} \omega_k(n)$, which provides an estimation of the firing rate of neuron k (it is independent of time from the stationarity assumption). If f is a monomial $\omega_{k_1}(n_1)\dots\omega_{k_m}(n_m)$, $1 \leq n_1 \leq n_2 \leq n_m < T$, then $\pi_\omega^{(T)}[f] = \frac{1}{T-n_m} \sum_{n=0}^{T-n_m} \omega_{k_1}(n_1+n)\dots\omega_{k_m}(n_m+n)$, and so on. Why using the cumbersome notation $\pi_\omega^{(T)}[f]$? This is to remind the reader that such empirical averages are *random variables*. They fluctuate from one raster to another *i.e.*, $\pi_{\omega^{(1)}}^{(T)}[f] \neq \pi_{\omega^{(2)}}^{(T)}[f]$ for distinct rasters $\omega^{(1)}, \omega^{(2)}$. Moreover, those fluctuations depend on T .

Assume now that all empirical rasters have all been generated by an hidden Markov chain and additionally that this chain is ergodic with a Gibbs distribution μ . Then, all those rasters obey $\pi_{\omega^{(r)}}^{(T)}[f] \rightarrow \mu[f]$, $r = 1, \dots, \mathcal{N}$, as $T \rightarrow +\infty$, whatever f : the time average converges to the average with respect to the hidden probability μ (this is one of the definitions of ergodicity). As a consequence the fluctuations of the

time-average about the exact mean $\mu[f]$ tends to 0, typically like $\frac{K_f}{\sqrt{T}}$, where K_f is a constant depending on f . This is the celebrated central limit theorem stating moreover that fluctuations about the mean are Gaussian [23]. We come back to this point in Sect. 1.3.2.4.

The remarkable consequence of ergodicity (which implies stationarity) is that the empirical average can be estimated from one raster only. Now, if we have \mathcal{N} rasters available we can use them to enlarge artificially the sample size, *e.g.* computing empirical average by $\frac{1}{\mathcal{N}} \sum_{r=1}^{\mathcal{N}} \pi_{\omega^{(r)}}^{(T)}[f]$. This also allows the computation of error bars as well as more elaborated statistical estimation techniques [48].

What if the stationarity assumption is violated? Then, the average of f depends on time and one computes the empirical average from the \mathcal{N} rasters. We denote $\pi^{(\mathcal{N})}[f(n)]$ the average of f at time n , performed over \mathcal{N} rasters. For example when $f(\omega) = \omega_k(n)$, $\pi^{(\mathcal{N})}[f(n)] = \frac{1}{\mathcal{N}} \sum_{r=1}^{\mathcal{N}} \omega_k^{(r)}(n)$ is the sample-averaged probability that neuron k fires at time n . If all rasters are described by the same probability (the Gibbs distribution which is also defined in the non-stationary case), then $\pi^{(\mathcal{N})}[f(n)] \rightarrow \mu[f(n)]$ as $\mathcal{N} \rightarrow +\infty$.

1.3.2.4 Example of Empirical Average: Estimating Instantaneous Pairwise Correlations

Assume that spikes are distributed according to an hidden probability μ supposed to be stationary for simplicity. The instantaneous pairwise correlations of neurons k, j with respect to μ is:

$$C(k, j) = \mu[\omega_k(0)\omega_j(0)] - \mu[\omega_k(0)]\mu[\omega_j(0)]. \quad (1.11)$$

Since μ is stationary the index 0 can be replaced by any time index (time-translation invariance of statistics).

Assume now that we have a raster ω distributed according to μ . An estimator of $C(k, j)$ is:

$$C_{\omega}^{(T)}(k, j) = \pi_{\omega}^{(T)}[\omega_k(0)\omega_j(0)] - \pi_{\omega}^{(T)}[\omega_k(0)]\pi_{\omega}^{(T)}[\omega_j(0)]. \quad (1.12)$$

It converges to $C(k, j)$ as $T \rightarrow +\infty$.

The events "neuron k fires at time 0" ($\omega_k(n) = 1$) and "neuron j fires at time 0" ($\omega_j(n) = 1$) are *independent* if $\mu[\omega_k(0)\omega_j(0)] = \mu[\omega_k(0)]\mu[\omega_j(0)]$, thus $C(k, j) = 0$. (Note that independence implies vanishing correlation but the reverse is not true in general. Here the two properties are equivalent thanks to the binary 0, 1 form of the random variables $\omega_k(0), \omega_j(0)$).

Assume now that the observed raster has been drawn from a probability where these events are independent, but the experimentalist who analyzes this raster does not know it. To check independence she computes $C_{\omega}^{(T)}(k, j)$ from the experimental raster ω . However, since T is finite, $C_{\omega}^{(T)}(k, j)$ will not be exactly 0. More precisely, from the central limit theorem the following holds. The probability that the random variable $\left| C_{\omega}^{(T)}(k, j) \right|$ is larger than ϵ , is well approximated (for large T and small ϵ) by $e^{-\frac{\epsilon^2 T}{K}}$. K can be exactly computed (Sect. 1.3.1.5). In the simplest case where spikes are drawn independently with a probability p of having a spike, K is equal to $p^2(1-p^2)$. Thus, fluctuations are Gaussian and their mean-square deviation decay with T as $\sqrt{\frac{K}{T}}$. As a consequence, even if neuron j and k are independent, the quantity $C_{\omega}^{(T)}(k, j)$ will never be 0: it has *fluctuations* around 0.

This can be seen by a short computer program drawing at random 0's and 1's independently, with the probability p to have a '1', and plotting $C_{\omega}^{(T)}(k, j)$ for different values of ω , while increasing T (Fig. 1.6).

As a consequence, it is stricto-sensu not possible to determine whether random variables are uncorrelated, by only computing the empirical correlation from samples of size T , since even if these variables are uncorrelated, the empirical correlation will never be zero. There exist statistical tests of independence from empirical data, beyond the scope of this chapter. A simple test consists of plotting the empirical correlation versus T and check whether it tends to zero as $\sqrt{\frac{K}{T}}$. Now, experiments affords only sample of limited size, where T rarely exceeds 10^6 . So, fluctuations are of order $\sqrt{K} \times 10^{-3}$ and it makes a difference whether K is small or big.

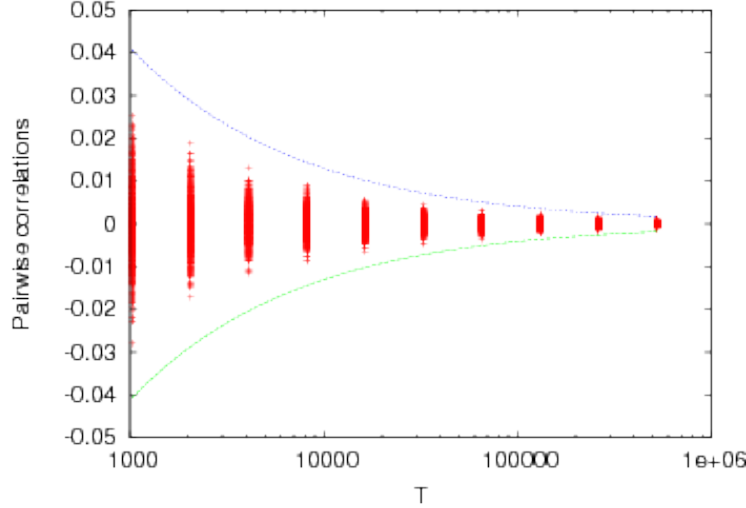


Fig. 1.6 Correlation (1.12) as a function of sample length T in a model where spikes are independent. For each T we have generated 1000 rasters of length T , with two independent neurons, drawn with a firing rate $p = \frac{1}{2}$. For each raster we have computed the pairwise correlation (1.12) and plotted it in log-scale for the abscissa (red point). In this way we have a view of the fluctuations of the empirical pairwise correlation about its (zero) expectation. The full lines represent respectively the curves $3\sqrt{\frac{p^2(1-p^2)}{T}}$ (blue) and $-3\sqrt{\frac{p^2(1-p^2)}{T}}$ (green) accounting for the Gaussian fluctuations of $C_\omega^{(T)}(k, j)$: 99% of the $C_\omega^{(T)}(k, j)$'s values lie between these two curves.

437 It is therefore difficult to interpret *weak* empirical correlations. Are they sample fluctuations of a
 438 system where neurons are indeed independent, or are they really significant, although weak? This issue
 439 is further addressed in Sect. 1.4.2.

440 1.3.2.5 Matching Experimental Averages

441 Assume that an experimentalist observes \mathcal{N} rasters, and assume that all those rasters are distributed
 442 according to an hidden probability distribution μ . Is it possible to determine or, at least, to approach μ
 443 from those rasters? One possibility relies on the maximal entropy principle described in the next sections.
 444 We assume for the moment that statistics is stationary.

445 Fix \mathcal{K} observables \mathcal{O}_k , $k = 1, \dots, \mathcal{K}$, and compute their empirical average $\pi_\omega^{(T)}[\mathcal{O}_k]$. The remarks
 446 of the previous sections hold: since all rasters are distributed according to μ , $\pi_\omega^{(T)}[\mathcal{O}_k]$ is a random
 447 variable with mean $\mu[\mathcal{O}_k]$ and Gaussian¹ fluctuations about its mean, of order $\frac{1}{\sqrt{T}}$. If there are $\mathcal{N} > 1$
 448 rasters the experimentalist can estimate the order of magnitude of those fluctuations and also analyze the
 449 raster-length dependence. *In fine*, she obtains an empirical average value for each observable, $\pi_\omega^{(T)}[\mathcal{O}_k] =$
 450 C_k , $k = 1, \dots, \mathcal{K}$. Now, to estimate the hidden probability μ , by some approximated probability μ_{ap} , she
 451 has to assume, as a minimal requirement, that:

$$\pi_\omega^{(T)}[\mathcal{O}_k] = C_k = \mu_{ap}[\mathcal{O}_k], \quad k = 1, \dots, \mathcal{K}, \quad (1.13)$$

452 *i.e.*, the expected average of each observable, computed with respect to μ_{ap} is equal to the average found
 453 in the experiment. This fixes a set of *constraints* to approach μ . We call μ_{ap} a *statistical model*.

Unfortunately, this set of conditions does not fix a unique solution but infinitely many! As an example if we have only one neuron whose firing rate is $\frac{1}{2}$, then a straightforward choice for μ_{ap} is the probability where successive spikes are independent ($P[\omega_k(n)\omega_k(n-1)] = P[\omega_k(n)]P[\omega_k(n-1)]$) and where the probability of a spike is $\frac{1}{2}$. However, one can also take a one-step memory model where transition probabilities obey $P[\omega_k(n) = 0 | \omega_k(n-1) = 0] = P[\omega_k(n) = 1 | \omega_k(n-1) = 1] = p$, $P[\omega_k(n) = 0 | \omega_k(n-1) = 1] = P[\omega_k(n) = 1 | \omega_k(n-1) = 0] = 1 - p$, $p \in [0, 1]$. In this case, indeed the invariant probability of the corresponding Markov chain is $\mu_{ap}[\omega_k(n) = 0, 1] = \frac{1}{2}$, since from Eq. (1.5),

¹ Fluctuations are not necessarily Gaussian, if the system undergoes a second order phase transition where the topological pressure introduced in Sect. 1.3.1.5 is not twice differentiable.

$$\begin{aligned} \mu_{ap}[\omega_k(n) = 0] &= \sum_{\omega_k(n-1)=0,1} P[\omega_k(n) = 0 | \omega_k(n-1)] \mu_{ap}[\omega_k(n-1)] \\ &= \left(\frac{p}{2} + \frac{1-p}{2} \right) = \frac{1}{2}. \end{aligned}$$

454 The same holds for $\mu_{ap}[\omega_k(n) = 1]$. In this case, we match the constraint too but with a model where
 455 successive spikes are *not* independent. Now, since p takes values in the interval $[0, 1]$ there are uncountably
 456 many Markov chains with memory depth 1 matching the constraint. One could also likewise consider
 457 memory depth $D = 2, 3$ and so on.

458
 459 Since transition probabilities reflect the underlying (causal) mechanisms taking place in the observed
 460 of the neural network, the choice of the statistical model defined by those transition probabilities is
 461 not anecdotal. In the example above, that can be easily generalized, one model considers that spikes
 462 are emitted like a coin tossing, without memory, while other models involve a causal structure with a
 463 memory of the past. Even worse, there are infinitely many choices for μ_{ap} since (i) the memory depth
 464 can be arbitrary; (ii) for a given memory depth there are (infinitely) many Markov chains whose Gibbs
 465 distribution matches the constraints (1.13). Is there a way to selecting, *in fine*, only one model from
 466 constraints (1.13), by adding some additional requirement? The answer is "yes".

467 1.3.2.6 Entropy

468 The entropy rate or Kolmogorov-Sinai entropy of a *stationary* probability distribution μ is:

$$h[\mu] = - \lim_{n \rightarrow \infty} \frac{1}{n} \sum_{\omega_1^n} \mu[\omega_1^n] \log \mu[\omega_1^n], \quad (1.14)$$

469 where the sum holds over all possible blocks ω_1^n . This definition holds for systems with finite or infinite
 470 memory. In the case of a Markov chain with memory depth $D > 0$, we have [12]

$$h[\mu] = - \sum_{\omega_1^{D+1}} \mu[\omega_1^{D+1}] P[\omega(D+1) | \omega_1^D] \log P[\omega(D+1) | \omega_1^D], \quad (1.15)$$

471 Note that, from time-translation invariance the block ω_1^D can be replaced by ω_n^{D+n-1} , for any integer n .

472 When $D = 0$, the entropy reduces to the classical definition:

$$h[\mu] = - \sum_{\omega(0)} \mu[\omega(0)] \log \mu[\omega(0)]. \quad (1.16)$$

473 1.3.2.7 Gibbs Distributions in the Stationary Case

474 In the stationary case Gibbs distributions obey the following variational principle [57, 28, 10]:

$$\mathcal{P}(\phi) = \sup_{\nu \in \mathcal{M}_{inv}} (h[\nu] + \nu[\phi]) = h[\mu] + \mu[\phi], \quad (1.17)$$

475 where \mathcal{M}_{inv} is the set of all possible stationary probabilities ν on the set of rasters with N neurons; $h[\nu]$
 476 is the entropy of ν and $\nu[\phi]$ is the average value of ϕ with respect to the probability ν . Looking at the
 477 second equality, the variational principle (1.17) selects, among all possible probability ν , *one* probability
 478 which realizes the supremum, the Gibbs distribution μ .

479 The quantity $\mathcal{P}(\phi)$ is called the *topological pressure*. For a normalized potential it is equal to 0. How-
 480 ever, the variational principle (1.17) holds for non-normalized potentials as well *i.e.*, functions which are
 481 not the logarithm of a probability [57, 28, 10].

482

483 In particular, consider a function of the form:

$$\mathcal{H}_\beta(\omega_{-D}^0) = \sum_{k=1}^{\mathcal{K}} \beta_k \mathcal{O}_k(\omega), \quad (1.18)$$

484 where \mathcal{O}_k are observables, β_k real numbers and β denotes the vector of β_k 's, $k = 1, \dots, \mathcal{K}$. We assume
 485 that each observable depends on spikes in a time interval $\{-D, \dots, 0\}$.

486 To the non-normalized potential $\mathcal{H}_\beta(\omega_{-D}^0)$ one can associate a normalized potential ϕ of the form:

$$\phi(\omega_{-D}^0) = \mathcal{H}_\beta(\omega_{-D}^0) - \log \zeta_\beta(\omega_{-D}^0), \quad (1.19)$$

487 where $\zeta(\omega_{-D}^0)$ is a function that can explicitly computed. In short, one can associate to the potential
 488 $\mathcal{H}_\beta(\omega_{-D}^0)$ a matrix with positive coefficient; $\zeta_\beta(\omega_{-D}^0)$ is a function of the (real positive) largest eigenvalue
 489 of this matrix as well as of the corresponding right eigenvector (see [74] for details). This function depends
 490 on the model-parameters β . The topological pressure is the logarithm of the largest eigenvalue.

491 In this way, \mathcal{H}_β defines a stationary Markov chain with memory depth D , with transition probabilities:

$$P[\omega(0) | \omega_{-D}^{-1}] = \frac{e^{\mathcal{H}_\beta(\omega_{-D}^0)}}{\zeta_\beta(\omega_{-D}^{-1})}. \quad (1.20)$$

492 Denote μ_β the Gibbs distribution of this Markov chain. The topological pressure $\mathcal{P}(\phi_\beta)$ obeys:

$$\frac{\partial \mathcal{P}(\phi_\beta)}{\partial \beta_k} = \mu_\beta[\mathcal{O}_k], \quad (1.21)$$

493 while its second derivative controls the covariance of the Gaussian matrix characterizing the fluctuations
 494 of empirical averages of observables about their mean. Note that those fluctuations are Gaussian if the
 495 second derivative of \mathcal{P} is defined. This holds if all transitions probabilities are positive.

496 In the memory-less case $D = 0$ where only the statistics of instantaneous spiking patterns is considered,
 497 the Gibbs distribution reads:

$$\mu_\beta(\omega(0)) = \frac{e^{\mathcal{H}_\beta(\beta, \omega(0))}}{\sum_{\omega(0)} e^{\mathcal{H}_\beta(\beta, \omega(0))}}. \quad (1.22)$$

498 In this case,

$$\zeta_\beta = \sum_{\omega(0)} e^{\mathcal{H}_\beta(\beta, \omega(0))}. \quad (1.23)$$

499 This is a constant (it does not depend on the raster). It is called *partition function* in statistical physics.

500

501 1.3.2.8 The Maximal Entropy Principle

502 Assume now that we want to approximate the exact (unknown) probability μ by an approximated prob-
 503 ability μ_{ap} that matches the constraints (1.13). The idea is to take as a statistical model μ_{ap} the Gibbs
 504 distribution of a function of the form (1.18), corresponding to a set of constraints attached to observables
 505 \mathcal{O}_k , where the β_k 's are free parameters of the model. Thus, the statistical model is fixed by the set of
 506 observables and by the value of β . We write then, from now on, μ_β instead of μ_{ap} .

507 Looking at the variational principle (1.17), we have to take the supremum over all probabilities ν that
 508 matches (1.13), *i.e.*, $\mu_\beta[\mathcal{O}_k] = C_k$ so that $\mu_\beta[\mathcal{H}_\beta]$ is a constant for fixed β . Therefore, in this case (1.13)
 509 reduces to *maximizing the entropy rate given the constraints* (1.13). This the classical way of introducing
 510 Gibbs distributions in physics courses. Then, the β_k 's appear as Lagrange multipliers, that have to be
 511 tuned to match (1.13). This can be done thanks to (1.21). Note that the topological pressure is convex
 512 so that the solution of (1.21) is unique.

513

514 The important point is that procedure provides a *unique* statistical model defined by the transition
 515 probabilities (1.20). Thus, we have solved the degeneracy problem of Sect. 1.3.2.5 in the stationary case.

516 1.3.2.9 Range-1 Potentials

517 Let us now present a few examples used in the context of spike train analysis of MEA data, among others.

518 The easiest examples are potentials with a zero memory depth, in the stationary case, where therefore
519 the spiking pattern $\omega(0)$ is independent of $\omega(-1)$. This corresponds to *range-1 potentials*.

520 Among them, the simplest potential has the form:

$$\phi_\beta(\omega(0)) = \sum_{k=1}^N \beta_k \omega_k(0) - \log(\zeta_\beta). \quad (1.24)$$

521 It corresponds to impose constraints only on firing rates of neurons. We have $\zeta_\beta = \prod_{k=1}^N (1 + e^{\beta_k})$ and
522 the corresponding Gibbs distribution is easy to compute:

$$\mu[\omega_m^n] = \prod_{l=m}^n \prod_{k=1}^N \frac{e^{\beta_k \omega_k(l)}}{1 + e^{\beta_k}}. \quad (1.25)$$

Thus, the corresponding statistical model is such that spikes are independent. We call it a *Bernoulli model*. The parameter β_k is directly related to the firing rate r_k since $r_k = \mu(\omega_k(0) = 1) = \frac{e^{\beta_k}}{1 + e^{\beta_k}}$, so that we may rewrite (1.25) as:

$$\mu[\omega_m^n] = \prod_{l=m}^n \prod_{k=1}^N r_k^{\omega_k(l)} (1 - r_k)^{1 - \omega_k(l)},$$

523 the classical probability of coin tossing with independent probabilities.

524
525 Another prominent example of range-1 potential is inspired from statistical physics of magnetic systems
526 and has been used by Schneidman and collaborators in [60] for the analysis of retina data (Sect. 1.4). It
527 is called *Ising potential* and reads, with our notations:

$$\phi(\omega(0)) = \sum_{k=1}^N \beta_k \omega_k(0) + \sum_{1 \leq j < k \leq N} \beta_{kj} \omega_k(0) \omega_j(0) - \log \zeta_\beta. \quad (1.26)$$

528 The corresponding Gibbs distribution provides a statistical model where synchronous pairwise synchrono-
529 nizations $\omega_k(0)\omega_j(0)$ between neurons are taken into account, but neither higher order spatial correlations
530 nor other time correlations are considered. The function ζ_β is the classical partition function (1.23).

531 The Ising model is well known in statistical physics and the analysis of spike statistics with this
532 type of potential benefits from a diversity of methods leading to really efficient algorithms to obtain the
533 parameters β from data ([71, 51, 55, 11]).

534 1.3.2.10 Markovian Potentials

535 Let us now consider potentials of the form (1.7) allowing to consider spatial dependence as well as time
536 dependence upon a past of depth D .

537 Consider first a stationary Markov chain with memory depth 1. The potential has the form:

$$\phi(\omega_{-1}^0) = \sum_{k=0}^{N-1} \beta_k \omega_k(0) + \sum_{k=0}^{N-1} \sum_{j=0}^{k-1} \sum_{\tau=-1}^0 \beta_{kj\tau} \omega_k(0) \omega_j(\tau) - \log \zeta_\beta(\omega(-1)). \quad (1.27)$$

538 This case has been investigated in [34] for spike train analysis of spike trains in the parietal cat cortex,
539 assuming stationarity.

540
541 All examples treated above concerns stationary situations. In the non-stationary case, the entropy rate
542 is not defined and the Gibbs distributions cannot be defined via the maximal entropy principle, while it
543 is still possible to define them as done in Sect. 1.3.1.5. Now, the most general form for non-stationary
544 Markov chain with memory depth D corresponds to potentials of the form:

$$\phi_n(\omega_{n-D}^n) = \sum_{l=-D}^0 \sum_{\mathcal{P}(N,D)} \beta_{i_1, n_1, \dots, i_l, n_l}(n) \omega_{i_1}(n+n_1) \dots \omega_{i_l}(n+n_l), \quad (1.28)$$

545 where the sum $\sum_{\mathcal{P}(N,D)}$ holds on the set of non repeated pairs of integers (i, n) with $i \in \{1, \dots, N\}$ and
 546 $n \in \{-D, \dots, 0\}$. Indeed, it can be shown that any function of blocks with depth D , $f(\omega_{n-D}^n)$ can be
 547 written as a linear combination of all possible monomials, a polynomial, constructed on blocks of depth
 548 D [25]. In the non-stationary case the coefficients $\beta_{i_1, n_1, \dots, i_l, n_l}(n)$ depend explicitly on n . They can be
 549 chosen so that (1.28) is normalized.

550 1.3.2.11 Non-Markovian Potentials

551 One can conceptually extend the definition of Markovian potentials to the case when $D \rightarrow -\infty$. This
 552 corresponds to a process with an infinite memory called “chain with complete connections” which is
 553 widely studied in the mathematical and mathematical physics literature (see [33] for a review). In this
 554 case the potential is a “function” $\phi_n(\omega_{-\infty}^n)$ depending on a infinite past $\omega_{-\infty}^{n-1}$. Although this case seems
 555 rather abstract, it turns out that the only known examples where spike train statistics can be exactly
 556 characterized in neural networks models are of this form. An example is given below. Moreover, this
 557 potential form allows to recover all the examples above.

558 1.3.2.12 How Good is the Estimation?

559 Once we have chosen a set of constraints and once we have found the parameters β to match (1.13), how
 560 can we check the goodness of the model? Additionally, changing the set of constraints provides another
 561 model. How can we compare two statistical models?

562 There is a wide literature in statistics dealing with the subject. In the realm of spike train analysis an
 563 important reference is [48] and references therein. Here, we point out two criteria for model comparison,
 564 used in this chapter as an illustration.

565
 566 A first and straightforward criterion consists of computing the empirical probability of blocks of depth
 567 $1, 2, \dots$ and to compare it to the probability predicted by the model. Of course, the number of blocks of
 568 depth R increases like 2^{NR} ; moreover the probability of large blocks is expected to decrease fast with the
 569 block depth. So, practically, one considers a subset of possible blocks. The challenge is in fact to predict
 570 the probability of events which have not been included as constraints in the Gibbs potential of the model.
 571 For example, does an Ising model well predict the probability of occurrence of triplets, quadruplets, of
 572 non simultaneous spikes?

573 The typical representation of this criterion is a graph, with, on abscissa, the observed probability
 574 of blocks and, on ordinate, the predicted probability. Thus, to each block corresponds a point in this
 575 two-dimensional graph. A “good” model is such that all points spread around the diagonal $y = x$. The
 576 distance to the diagonal is expected to increase as the probability of the block decreases thanks to the
 577 central limit theorem. Indeed, if the exact probability of a block is P , then the empirical estimation of
 578 this probability is a random variable with a Gaussian distribution, of mean P , and a variance that can
 579 be computed from the topological pressure. A usual approximation of this variance is $P(1 - P)$. Thus,
 580 in a similar way as in Fig. 1.6, the set of points in the graph spreads around the diagonal in a region
 581 delimited by the curves $\pm 3\sqrt{\frac{P(1-P)}{T}}$ called “confidence bounds”. An example is given in Fig. 1.7.

582
 583 Another criterion is provided by the *Kullback-Leibler divergence (KL)* which provides some notion
 584 of asymmetric “distance” between two probabilities. Its computation is numerically delicate but, in the
 585 present context of Gibbs distributions, the following holds. If μ is the hidden (time-translation invariant
 586 probability) and μ_β a Gibbs distribution with a potential ϕ_β , one has, [28, 10]:

$$d(\mu, \mu_\beta) = \mathcal{P}(\phi_\beta) - \mu[\phi_\beta] - h(\mu). \quad (1.29)$$

587 This allows in principle to estimate the divergence of our model to the hidden probability μ , providing
 588 the exact spike train statistics. The smaller $d(\mu, \mu_\beta)$ the better is the model. Unfortunately, since μ is
 589 unknown this criterion looks useless. However, from 1.3.2.3, $\mu[\phi_\beta]$ is well approximated by $\pi_\omega^{(T)}[\phi_\beta]$

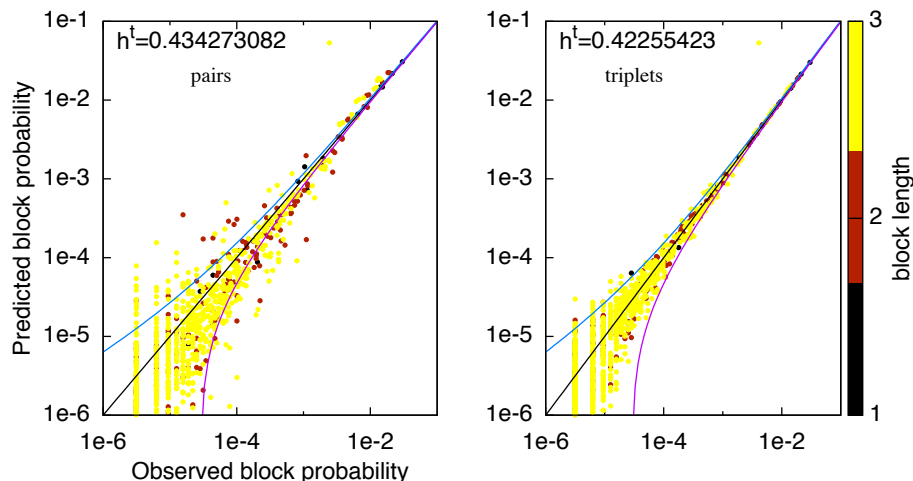


Fig. 1.7 Analysis of salamander retina data, from [74]. The estimated block probability versus the observed block probability for all blocks from range 1 to 4 (coded by colors), for $N = 4$ neurons with a model of range $R = 3$ for pairs and triplets. We include the equality line $y = x$ and the confidence bounds (black lines) for each model, corresponding to $\pi^{(T)}(w) \pm 3\sigma_w$ with σ_w being the standard deviation for each estimated probability given the total sample length $T \sim 3 \cdot 10^5$. In the figure h^t corresponds to \tilde{h} , Eq. (1.30).

590 which can be computed from the raster. Additionally, the entropy $h(\mu)$ is unknown and its estimation
 591 by numerical algorithms for a large number of neurons is delicate [68]. However, when considering two
 592 statistical models $\mu_{\beta_1}, \mu_{\beta_2}$ with potentials $\phi_{\beta_1}, \phi_{\beta_2}$ to analyze the *same* data, $h(\mu)$ is a constant (it only
 593 depends on data). Thus, comparing these two models amounts to comparing $P[\phi_{\beta_1}] - \pi_{\omega}^{(T)}[\phi_{\beta_1}]$ and
 594 $P[\phi_{\beta_2}] - \pi_{\omega}^{(T)}[\phi_{\beta_2}]$. Thus, the quantity

$$\tilde{h}[\phi] = P[\phi] - \pi_{\omega}^{(T)}[\phi], \quad (1.30)$$

595 provides a relative criterion to compare models, *i.e.*, determining if model ϕ_{β_2} is significantly “better”
 596 that model ϕ_{β_1} , reduces to the condition:

$$\tilde{h}[\phi_{\beta_2}] \ll \tilde{h}[\phi_{\beta_1}]. \quad (1.31)$$

597 Its computation is detailed in [75, 74].

598 1.4 Using Gibbs Distributions to Analysis Spike Trains Statistics

599 In this section we show how the statistical tools presented in this chapter can be used to analyze spike
 600 trains statistics. In the “challenge” section we mention the current controversy about the question: Are
 601 G cells sensors independent encoders or, on the opposite, are neural correlations important for coding?
 602 We present here recent works where Gibbs distributions has been be used to address this question with
 603 important implications on neural coding. However, as we show, those examples also raise additional and
 604 fundamental questions. Some of them that can be addressed on theoretical grounds, by studying neural
 605 networks models. A third section presents an example of such a model where spike trains is known to have
 606 a Gibbs statistics and where the potential is explicitly known. We compare those results to the current
 607 state of the art in spike train analysis with Ising distributions.

608 1.4.1 Are Ganglion Cells Independent Encoders?

609 This question can be now reformulated in the context of Gibbs distributions. Independence between
 610 neurons means that spike statistics is described by a potential, possibly non-stationary, of the form:

$$\phi_n(\omega) = \sum_{k=1}^N \phi_{n,k}(\omega_k). \quad (1.32)$$

This assumption can be stated independently on the memory depth, so we write here $\phi_n(\omega)$ instead of $\phi_n(\omega_n^{n-D})$ to alleviate notations and to be as generic as possible. In (1.32) ω_k is the spike train $\{\omega_k(l)\}_{l \leq n}$ produced by neuron k only. In this way the transition probabilities of the global network are products of transition probability for each neuron and the Gibbs distribution (1.5) is a product of marginal distributions for one neuron. On the opposite, if one believes that spike correlations play an important role in statistics one has to include them in the Gibbs potential. Typically, spike correlations are characterized by monomials and the potential takes the generic form (1.28). Obviously, there are many possible choices for this potential, depending on the set of observables assumed to be relevant.

To compare different models one can use the criteria described in Sect. 1.3.2.12. Does an independent model predicts correctly the spike blocks occurring in the observations? If not, which correlations has to be included? How evolves the Kullback-Leibler divergence as the type of correlations (monomials) taken into account growth?

However, the application of those criteria is delicate in experimental data, taking into account the large number of cells, their different types and the relatively small size of spike train samples obtained from experiments. For these reasons analysis of retina data has been performed either for memory-less models where the number of neurons can be up to 100 neurons, or to models with memory with small range and a small number of neurons. Let us present some of those works.

1.4.2 Weak-Pairwise Correlations Imply Strongly Correlated Network States in a Neural Population.

A breakthrough in spike train analysis has been made by the seminal paper of E. Schneidman and collaborator [60]. They have considered carefully instantaneous pairwise spike correlations in experiments on the vertebrate retina. It appears that, mostly, those correlations are *weak*. But are they *significant*? In Sect. 1.3.2.4 we have shown that weak correlations can be hardly interpretable without further analysis. The maximal entropy principle provides a way to quantify the role of those correlations. Take a statistical model (a Gibbs potential) without constraint on instantaneous pairwise spike correlations, and fix only constraints on rates. This provides a Bernoulli model with a potential (1.24). Take another model where pairwise correlations are taken into account (but no higher-order interactions). This is an Ising model with potential (1.26). The authors compare those two models using the comparison between estimated block probability versus the observed block probability for *spatial* blocks, but also some other criteria such as the probability of having n spiking G cells in a time window of 20 ms.

Their work convincingly shows that although pairwise correlations are *weak*, they are nevertheless *necessary* to characterize spike trains statistics. The Ising model clearly does quite better than a Bernoulli model and the authors claim to “predict” about 90% of the multi spiking structure of a large G cells population in salamander and guinea pig. Note however that they focus on spatial pattern. This shows that weak correlations between pairs of neurons coexist with strongly collective behavior in the responses of ten or more neurons. Similarly, Shlens *et al.*[65] predict 99% of a complete ON and OFF parasol G cells population in primates with a Ising model . This suggests that the neural code is dominated by correlation effects.

On the other hand, this work does not directly unravel the importance of neural correlation for carrying information. Moreover, in [54], it has been shown that although Ising model is good for small populations, this is an artifact of the way data is binned and of the small size of the system. Additionally, it might be questionable whether more general forms of Gibbs distributions (*e.g.* involving more general monomials) could improve the estimation and account for deviations to Ising-model ([66, 71, 42]) and provide a better understanding of the neural code from the point of view of the maximal entropy principle [27]. Very recently, Ganmor and collaborators [19] have extended the maximal entropy principle introducing higher order *instantaneous* spikes correlations. Triplets and so on are considered although all spikes arise at the same time. This therefore still corresponds to a memory-less model. These authors have convincingly shown that such model describes more accurately retina responses to natural images than Ising model. In particular spatio temporal patterns were well predicted: binary words of 10 retinal G cells over 10 time steps. Note however that those data are binned (Sect. 1.5.1 for a definition and a discussion).

661 As a matter of fact, back to 1995, [36] already considered multi-unit synchronizations and proposed
 662 several tests to understand the statistical significance of spike synchronizations. A few years later, [35]
 663 generalized this approach to arbitrary spatio-temporal spike patterns and compared this method to other
 664 existing estimators of high-order correlations or Bayesian approaches. More recently, several papers have
 665 pointed out the importance of temporal patterns of activity at the network level [31, 76, 63]. As a
 666 consequence, a few authors ([34, 2, 53]) have attempted to define time-dependent Gibbs distributions on
 667 the base of a Markovian approach, but with one time step memory only, and under assumptions such as
 668 detailed balance, [34] or conditional independence between neurons, see Eq. (1) in [52]. A more general
 669 method relying on Gibbs distributions has been proposed in [75], and applied to the same data as [60],
 670 in [74]. The results shows a clear increase in the model accuracy (measured with the KL divergence 1.29)
 671 when adding *spatio-temporal* constraints.

672 In some sense, it is clear that the more parameters (or constraints) the more the model fits the data, up
 673 to some limit, fixed by the data and especially the raster size, where models become indistinguishable. Is
 674 there a minimal statistical model? A related question is: what does a statistical model teach us about the
 675 underlying neural network (*e.g.*, the retina) and about neural coding? Let us first present an important
 676 work addressing the second question, before addressing the first one.

677 1.4.3 The Architecture of Functional Interaction Networks in the Retina

678 A critical question to elucidating the neural code, at least from a theoretical point of view, is to confront
 679 multi-electrodes real data against sophisticated statistical models testing for the underlying neural struc-
 680 ture involved. Since the connectivity of any neural network can in principle growth exponentially as a
 681 function of the number of neurons, classical numerical methods can rapidly become inefficient. The work
 682 of Schneidman and collaborators [60] has nevertheless suggested that although the number of possible
 683 activity patterns and underlying interactions is exponentially large in a neural network, a pairwise-based
 684 Ising model gives a surprisingly accurate description of neural population activity patterns. So, an eco-
 685 nomical assumption to reducing a putative network dimensionality, is to use a pairwise correlation model
 686 able to recover the main network structure involved in the encoding of a natural movie [60].

687 More recently, searching for further reduction on the dimensionality of the network structure, Ganmor
 688 *et al.*[18] have shown the presence of small groups of neurons having strong correlated activity. As an
 689 outcome of their MEA spike train analysis the authors introduce the notion of *functional connectivity*.
 690 This corresponds to associating with the parameters in the Gibbs potential a network of "effective"
 691 interactions (β_{ij} for spike pairs, β_{ijk} for triplets, ...).

692 The performance of their model is clearly higher than when assuming independence between neu-
 693 rons. It is able to predict the neural activity, including synchrony, for larger neural networks as in [60]
 694 and the contribution of small groups of neurons to the complete population activity. To further reduce
 695 the structure of the network to most critical neural interactions, the authors apply a nearest-neighbors
 696 paradigm. An interesting result is that the reduction of close to 50% of the original pairwise interactions
 697 does not change the accuracy of predictions, and models most functional groups of nearest neurons with
 698 an accuracy $> 95\%$. Additionally, small functional overlapping units (10-20 neurons) seem to be a critical
 699 structure for the encoding of natural movies stimulus.

700 This work, together with [19], shows that a Gibbs potential with a relatively small number of pa-
 701 rameters, corresponding to effective interactions between neurons, is able to reproduce spike trains of
 702 populations of neurons in the retina submitted to natural images. The network of these effective interac-
 703 tions is organized in a hierarchical and modular manner so that large network models can be constructed
 704 from smaller sub-networks in a modular fashion. Thus, by a suitable scaling of parameters, one could be
 705 able to extrapolate the Gibbs potential of a small population of neurons to large populations. Moreover,
 706 in some sense, this effective network "underlies the code", from the terminology of the authors. This
 707 means that the spike generation, as a response to a stimulus (an image), results from a dynamical process
 708 which can be summarized by the Gibbs potential of the model.

709 This work raises however several questions. First, the potential considered by the authors is memory-
 710 less. No time dependent process takes place in the potential. In some sense, the time-causality expected
 711 in a neural network is hidden by the effective potential. Another critical aspect is the interpretation of
 712 the effective interaction. It is stated in [18] that "although the pairwise interactions in the model do
 713 not necessarily reflect a physical interaction between cells, they give a unique functional interaction map
 714 between the neurons in the network and represent statistical dependence between pairs of units." But, if

715 they do not represent physical interactions (synapses), what do these functional interactions correspond
716 to? To our knowledge this question has not been yet resolved.

717 1.4.4 Spike Train Analysis in a Neural Network Model

718 The maximal entropy principle relies on the assumption of stationarity as well as an *a priori* and some-
719 what *ad hoc* choice of observables. This choice severely constrains the form of the statistical model and
720 the information that can be extracted about the underlying neuronal network producing the spike. In
721 particular, the choice of observables determines the transition probabilities and implicitly fixes a causal
722 structure to analyze spike events. Especially, memory-less models focuses on synchronous events, hiding
723 somewhat temporal causality.

724 Obviously, it is extremely difficult to obtain a clear cut characterization of spike trains statistics from
725 experimental data, taking into account the experimental set up, spike acquisition, spike sorting, but
726 also the relatively small size of spike trains (typically, in retina experiments $T < 10^{5-6}$). So, a natural
727 question is: "Can one have a reasonable idea of what spike statistics could be in neural network *model*?"
728 The answer is "yes".

729 In neural networks spikes result from the collective and non linear dynamics of neurons coupled by
730 synapses (electrical or chemical) and submitted to "external" stimuli. As a consequence statistics of
731 spike train is closely related to this network structure (neurons and synapses characteristics) and to
732 the stimulus. The idea is to show here the relationships between the neural network structure and the
733 form of transition probabilities in an explicit example, a conductance-based neural network model of
734 Integrate-and-Fire (IF) type called "generalized Integrate and Fire" (gIF) and introduced by Rudolph
735 and Destexhe [56]. This section summarizes the paper [7].

736 1.4.4.1 The Model

737 We consider the evolution of a set of N neurons. Here, neurons are considered as "points" instead of
738 spatially extended and structured objects. As a consequence, we define, for each neuron $k \in \{1 \dots N\}$, a
739 variable $V_k(t)$ called the "membrane potential of neuron k at time t " without specification of which part
740 of a real neuron (axon, soma, dendritic spine, ...) it corresponds to.

741 Fix a firing threshold θ . The sub-threshold dynamics of the model is:

$$742 C_k \frac{dV_k}{dt} + g_k(t, \omega) V_k = i_k(t, \omega). \quad (1.33)$$

743 C_k is the membrane capacity. $g_k(t, \omega)$ is the integrated conductance at time t given the past spike activity
744 encoded in the raster ω . It is defined in the following way. Denote $\alpha_{kj}(t - \tau)$ the synaptic response of
745 neuron k , at time t , to a pre-synaptic spike from neuron j that aroused at time τ . Classical examples of
746 synaptic responses are $\alpha_{kj}(t) = e^{-\frac{t}{\tau_{kj}}} H(t)$ or $\alpha_{kj}(t) = \frac{t}{\tau_{kj}} e^{-\frac{t}{\tau_{kj}}} H(t)$, where H the Heaviside function
747 (that mimics causality) and τ_{kj} is the characteristic decay times of the synaptic response. In gIF model
748 the conductance $g_k(t, \omega)$ integrates the synaptic responses of neuron k to spikes arising in the past. Call
749 $t_j^{(r)}(\omega)$ the r -th spike-time emitted by neuron j in the raster ω , namely $\omega_j(n) = 1$ if and only if $n = t_j^{(r)}(\omega)$
for some r . Then,

$$750 g_k(t, \omega) = g_{L,k} + \sum_{j=1}^N G_{kj} \alpha_{kj}(t, \omega), \quad (1.34)$$

751 where $\alpha_{kj}(t, \omega) = \sum_{t_j^{(r)}(\omega) < t} \alpha_{kj}(t - t_j^{(r)}(\omega))$ sums up the spike responses of post-synaptic neuron k
752 to spikes emitted by the pre-synaptic neuron j at times $t_j^{(r)}(\omega) < t$. $g_{L,k}$ is the leak conductance of neuron
753 k .

754 Returning to Eq. (1.33) the term $i_k(t, \omega)$ is a current given by $i_k(t, \omega) = g_{L,k} E_L + \sum_{j=1}^N W_{kj} \alpha_{kj}(t, \omega) +$
755 $i_k^{(ext)}(t) + \sigma_B \frac{dB_k}{dt}$, where E_L is the Nernst leak potential, W_{kj} is the synaptic weight from j to k , $i_k^{(ext)}(t)$
the (time-dependent) external stimulus received by neuron k , and dB_k is a Brownian noise whose variance

756 is controlled by σ_B .

757
758 As in all IF models, when V_k reaches the firing threshold θ , it is reset. Here, however, it is not
759 instantaneously reset to a constant value, but to a Gaussian random variable with mean zero and variance
760 σ_R^2 , after a time delay $\delta > 0$ including the depolarization-repolarization and refractory period. We call
761 $\tau_k(t, \omega)$ the *last time before t where neuron k has been reset*.

762 1.4.4.2 Membrane Potential Decomposition

763 Given the spike history of the network it is easy to integrate (1.33) and to find an explicit expression for
764 the membrane potential at time t . It depends on the past spike history ω . Denote $V_k(t, \omega)$ the membrane
765 potential at time t given the spike history before t . Set:

$$\Gamma_k(t_1, t_2, \omega) = e^{-\frac{1}{C_k} \int_{t_1}^{t_2} g_k(u, \omega) du}, \quad (1.35)$$

766 corresponding to the flow of (1.33). We have $V_k(t, \omega) = V_k^{(det)}(t, \omega) + V_k^{(noise)}(t, \omega)$,

$$V_k^{(det)}(t, \omega) = V_k^{(syn)}(t, \omega) + V_k^{(ext)}(t, \omega) \quad (1.36)$$

767 where

$$V_k^{(syn)}(t, \omega) = \frac{1}{C_k} \sum_{j=1}^N W_{kj} \int_{\tau_k(t, \omega)}^t \Gamma_k(t_1, t, \omega) \alpha_{kj}(t_1, \omega) dt_1, \quad (1.37)$$

768 is the synaptic interaction term which integrates the pre-synaptic spikes from the last time where neuron
769 k has been reset. Additionally,

$$V_k^{(ext)}(t, \omega) = \frac{1}{C_k} \left[g_{L,k} E_L + \int_{\tau_k(t, \omega)}^t i_k^{(ext)}(t_1) \Gamma_k(t_1, t, \omega) dt_1 \right], \quad (1.38)$$

770 contains the stimulus $i_k^{(ext)}(t)$ influence. Thus $V_k^{(det)}(t, \omega)$ contains the deterministic part of the membrane
771 potential. On the opposite, $V_k^{(noise)}(t, \omega)$ is the stochastic part of the membrane potential. This is a
772 Gaussian variable with mean zero and variance

$$\sigma_k^2(t, \omega) = \Gamma_k^2(\tau_k(t, \omega), t, \omega) \sigma_R^2 + \left(\frac{\sigma_B}{C_k} \right)^2 \int_{\tau_k(t, \omega)}^t \Gamma_k^2(t_1, t, \omega) dt_1. \quad (1.39)$$

773 The first term in the right-hand side comes from the reset of the membrane potential to a random value
774 after resetting. The second one is due the integration of synaptic noise from $\tau_k(t, \omega)$ to t .

775 1.4.4.3 Statistics of Raster Plots

776 It has been shown in [7] that the gIF model (1.33) has a unique Gibbs distribution with a *non-stationary*
777 potential:

$$\phi_n(\omega) = \sum_{k=1}^N \phi_{n,k}(\omega), \quad (1.40)$$

778 with,

$$\phi_{n,k}(\omega) \stackrel{\text{def}}{=} \omega_k(n) \log \pi(X_k(n-1, \omega)) + (1 - \omega_k(n)) \log(1 - \pi(X_k(n-1, \omega))). \quad (1.41)$$

779 Here

$$X_k(n-1, \omega) = \frac{\theta - V_k^{(det)}(n-1, \omega)}{\sigma_k(n-1, \omega)}, \quad (1.42)$$

780 and

$$\pi(x) = \frac{1}{\sqrt{2\pi}} \int_x^{+\infty} e^{-\frac{u^2}{2}} du. \quad (1.43)$$

781 As announced in the beginning of this section, the Gibbs potential that constraints spike statistics
 782 summarizes several contributions. The effect of the synaptic network structure, integrated over the past
 783 spike history as well as over the contribution of the stimulus (external current), also integrated over the
 784 past spike history, appears in the term $V_k^{(det)}(n-1, \omega)$. The synaptic noise and the reset to a random
 785 value, integrated over the history, depends on the term $\sigma_k(n-1, \omega)$. We insist that the result holds for
 786 a *time-dependent external current*, i.e., a *non-stationary dynamics*.

787 The potential exhibits therefore clearly the causal structure of spikes generation. The probability to
 788 have a spike at time n depends *explicitly* on synaptic weights, defining the neural network structure, and
 789 on the stimulus, via the external current. Moreover, it introduces a clear history dependence. Now, there
 790 are several important remarks.

- 791 1. The number of parameters on which spike train statistics depend is relatively small. It increases like
 792 a polynomial in the number on neurons, *e.g.*, at most N^2 synaptic weights.
- 793 2. Those parameters are physical parameters: the synaptic weights between neurons, the stimulus, plus
 794 physical characteristics of the neuron such as leak Nernst potential. Thus, the potential outlines a
 795 network which is not *effective*, as in Sect. 1.4.3, but is the *real* underlying network. Additionally, this
 796 potential is *non-linear* function of the synaptic weights and stimulus while Ising-like models are *linear*
 797 in the interactions.
- 798 3. The memory is mathematically infinite. In other words, to handle the spike statistics *exactly*, one has
 799 to consider a non-Markovian potential with an infinite history ($D \rightarrow -\infty$).

800 1.4.4.4 From Non-Markovian to Markovian Potentials

801 Since the dependence on the past decays exponentially fast, thanks to the exponential decay of synaptic
 802 response, it is possible to provide Markovian approximations of the potential (1.40). Basically, one trun-
 803 cates the synaptic response after a characteristic time D and performs a series expansion of the function
 804 (1.43), using the fact that the power of a monomial is the same monomial. So, the series becomes a poly-
 805 nomial, which provides a Markovian potential of the form (1.28). Here, the coefficients $\beta_{i_1, n_1, \dots, i_l, n_l}(n)$'s
 806 depend explicitly on the synaptic weights (network structure) as well as on the stimulus. Now, for N
 807 neurons and a memory depth D , the truncated potential contains 2^{ND} coefficients $\beta_{i_1, n_1, \dots, i_l, n_l}(n)$, while
 808 the exact ($D \rightarrow -\infty$) potential depends only on a polynomial number of parameters. This shows that,
 809 in this model, a potential of the form (1.28) induces a strong, and somehow pathological, redundancy.

810 Additionally, the truncated potential is *far from Ising, or more elaborated potentials used in exper-*
 811 *imental spike train analysis*. As we have seen most of these models are memory-less and non causal.
 812 Now, the best approximation of the potential (1.40) by a memory-less potential is . . . Bernoulli. This is
 813 because of the specific form of ϕ : a term $\omega_k(0)$ multiplied by a function of $\omega_{-\infty}^{-1}$. To have a memory-less
 814 potential one has to replace this function by a constant, giving therefore a Bernoulli potential. So, Ising
 815 model as well as memory less models are rather poor in describing the statistics of model (1.33). But,
 816 then, how can we explain the success of Ising model to analyze retina data? We return to this point in
 817 the conclusion section.

818 1.4.4.5 Are Neurons Independent?

819 For this model we can answer the question of neurons independence. The potential (1.40) is a sum
 820 over neurons, similarly to (1.32), but it has not the same form as (1.32). The difference is subtle but
 821 essential. While in (1.32) the potential of neuron k , ϕ_k depends upon the past via the spike-history ω_k
 822 of *neuron k only*, in (1.40) ϕ_k depends upon the past via the spike-history ω of the *entire network*. The
 823 factorization in (1.40) reflects only a conditional independence: if the past spike history of the network is
 824 fixed then the only source of randomness is the noise, which is statistically independent by hypothesis,
 825 for all neurons. So, there is nothing deep in the factorization (1.40). On the opposite, a factorization like
 826 (1.32) would reflect a deeper property. Neurons would somewhat be able to produce responses which are
 827 well approximated by a function of their own history only, although each neuron receives inputs from
 828 many other neurons. Considering the form of the potential ϕ , given by (1.41) there is no chance to obtain
 829 the strong factorization property (1.32) unless neurons are disconnected. This property could however

830 arise if the model obeys a mean-field theory as the number of neurons tends to infinity. This requires, in
 831 general, strong constraints on the synaptic weights (vanishing correlations), not necessarily realistic.

832 1.4.4.6 Links with the Retina

833 This model is not sufficient to describe the retina since it neglects the specific types of bipolar, horizontal
 834 and some amacrine cells that do not "fire". Additionally, it neglects electric synapses (gap junctions)
 835 playing an important role in the connectivity as shown in Fig. 1.1(b). Recent investigations show that
 836 the conditional factorization property (1.40) *disappear* in the presence of gap junctions, so that statistics
 837 is expected to be even more complex, with no independence at all (Cessac, Cofre, in preparation).

838 1.5 Conclusion

839 In this chapter we have attempted to give a short overview of recent questions related with the concept of
 840 spike train analysis. Taking as an example the case of the retina we have presented a summary of recent
 841 experimental progresses from MEA recording to spike train analysis. On the theoretical side, we have
 842 introduced a general formalism connecting spike train statistics to Markov chains and Gibbs distributions.
 843 This formalism looks appropriate since, on one hand it allows to recover the Gibbs distributions forms used
 844 currently in the literature of spike train analysis, and on the other hand it affords analytical developments
 845 to characterize spike train probabilities in neural networks models. Finally, we have presented three
 846 examples of recent successes in spike trains analysis. These examples are encouraging but raise salient
 847 questions that we would like now to address.

848 1.5.1 *Ising or not Ising?*

849 In Sect. 1.4.2, 1.4.3 we have outlined the relative success of Ising model to analyze retina data, while in
 850 Sect. 1.4.4.4 we have computed explicitly the potential and concluded that it is quite far from Ising. What
 851 is the reason of this discrepancy? A first explanation, exposed in Sect. 1.4.4.6, is that the model (1.33)
 852 is not a good model for the retina. Another possible reason is the difference of *time scales* considered in
 853 both approaches. While the theoretical results of Sect. 1.4.4 consider neurons dynamics at the time scale
 854 of a spike (about 1 ms), statistical analysis of experimental data use, in all the examples we know, *data*
 855 *binning*. From preliminary analyzes of spike train (correllograms), one extracts a characteristic time scale
 856 τ (about 10 – 20ms) from which spike trains are binned. Recall that a binned spike train is a raster Ω ,
 857 obtained by cutting the original raster ω into time-slices of size τ and setting $\Omega_k(n) = 1$ in the slice n
 858 if and only if neuron k as fired at least once in this slice. In this way, one smooths out the dynamical
 859 interactions occurring at a time scale smaller than τ (especially synaptic interactions). So the coefficient
 860 β_{kj} 's in a binned-Ising model with a binning of 10 – 20ms somewhat integrate the synaptic transmission
 861 effects and neurons pairwise interactions appear as instantaneous. In this way, one loses an important
 862 part of the dynamics and of the network structure. The "functional interactions" evoked in Sect. 1.4.3
 863 corresponds to an integration of physical interactions over the binning time scale. For example, in the
 864 Ising model, the pairwise coefficient β_{kj} integrates the effect of several circuits connecting neuron j to
 865 neuron k , as well as dynamic-dependent effects. As a matter of fact its interpretation is rather delicate.

866 This is however certainly not the end of the story and this aspect has to be still investigated on the
 867 theoretical and experimental side.

868 1.5.2 *Linear Potentials versus Combinatorial Explosion*

869 Experimental attempts to go "beyond Ising" [34, 73] suggest that Markovian models with increasing range
 870 should describe better and better the spike statistics. This is also expected from the theoretical analysis
 871 summarized in Sect. 1.4.4. However, this raises several remarks and questions. First, it is evident that the
 872 more parameters, the best is the model, but what do we learn from this plethora of parameters? Second,

873 one has to face the critical issue of an exponential increase of parameters, with the potential range and
 874 with the number of neurons, so that numerical methods can rapidly become inefficient. Moreover, the
 875 sample size required to determine those coefficients is expected to increase also exponentially, ruining any
 876 hope to extract reliable coefficients from empirical data. Finally, as outlined in the previous section, the
 877 interpretation of the coefficients is difficult even for the simplest pairwise interactions β_{kj} .

878 Our point of view is that the linear potential approach, based on the maximal entropy principle, is
 879 maybe inappropriate. On the opposite, non linear potentials of the form (1.40), truncated to a finite
 880 memory depend on a number of parameters, the physical parameters of the network, which increases
 881 only polynomially with the number of neurons. Although, the number of blocks determining the potential
 882 increases exponentially fast with the memory depth, it could well be that only a small proportion of blocks
 883 are sufficient to extract most of the information about the hidden parameters. Finally, the interpretation
 884 of parameters is here straightforward and such a model allows to treat the non-stationary case. This may
 885 provide an alternative to Ising-like models to study spike train statistics in experiments.

886 1.6 Outlook

887 In this section we would like to point out a few challenges for the next future, on the theoretical and
 888 experimental sides.

889 1.6.1 Gibbs Distributions and the Neural Code

890 Although interesting results have come out from the Gibbs analysis of retina spike trains, the link between
 891 spike statistics and their modeling with Gibbs distribution on one hand, and the way how a visual scene
 892 is encoded by G cells spikes emission on the other hand, remains rather tight. Defining a priori a Gibbs
 893 potential from a set of constraints superimposes upon spike trains a causal structure, purely spatial
 894 or spatio-temporal, associated with "effective interactions", *e.g.* the coefficients $\beta_{i_1, n_1, \dots, i_l, n_l}(n)$ in the
 895 polynomial expansion (1.28). What do these interactions teach us about the neural code? How are they
 896 related to a visual scene? Given a Gibbs distribution that fits well retina spike statistics is it possible to
 897 infer information about the visual scene perceived by this retina? Is it possible to build retina "decoders"
 898 from Gibbs statistics? If yes, does a "correlated decoder", with correlated G cells perform better than a
 899 "rate decoder" where G cells outputs are independent? Although interesting advances has been done on
 900 these questions (see, *e.g.*, [59]) we believe that they are far from being solved, and that they constitute
 901 a challenge for the next years.

902 A related question concerns the concept of receptive field. We have presented in Sect. 1.2.1.2 the
 903 classical notion of RF which is associated with an isolated G cell, *independently of what the neighboring*
 904 *G cells* are perceiving. Additionally, *e.g.* fig. 1.3, describes well the response of a G cell in terms of firing
 905 rates without need of considering higher order statistics. It is a current approach to model RF as filters,
 906 typically linear, followed by a non-linear correction [46]. How does the paradigm of linear-non linear
 907 filter connects with the paradigm of Gibbs distribution? Can we infer the shape of the RF filter from the
 908 Gibbs potential? Classical RF filters are based on firing rates for individual G cells; on the opposite Gibbs
 909 statistics deals with spike events (monomials) for collective behaviors. Are these two visions coherent? Is
 910 there a link *e.g.* between effective interactions and RF?

911 To our best knowledge those questions have not been resolved. On the theoretical side they can be
 912 addressed in the context of Gibbs distributions. Given a Gibbs potential modeling retina response it could
 913 be possible to compute the linear response to a stimulus considered as a weak perturbation of dynamics.
 914 This linear response is characterized by a convolution kernel which could be compared to the models of
 915 receptive field filters used in the literature. This work remains still to be done though.

916 1.6.2 Experimental Limits

917 To our opinion the current experimental set up is faced with the following limits.

- 918 • Natural stimulus must reproduce ecological environment, where animals lives, including the way how
919 animals explore it, how they are in action, moving their head and eyes. As a consequence the cap-
920 tured images used in experiments need to be dynamically displayed to the retina, reproducing natural
921 motions.
- 922 • Sophisticated experiment require MEA devices recording from a large numbers of cells (*e.g.*> 100).
923 For example a new MEA technology using 4096 electrodes matrix makes it possible to recording most
924 of the neurons in a single small surface, but the recording data string would take several gigabytes of
925 saving space and requires fast technologies to access data. Moreover, their numerical analysis, spike
926 sorting + spike train analysis, in any computer or even a cluster will take a very long time. Actually,
927 • The MEA outputs need adequate spike sorting algorithms able to deal with larger and larger numbers
928 of cells. Current algorithms allow to treat about 200 electrodes signals.
- 929 • Spike train analysis necessitates adequate statistical tools applying to a large number of interacting cells
930 to evaluate different possible models for neural encoding (*e.g.* population coding). Current algorithms
931 allow to treat less than 100 neurons for an Ising model.
- 932 • A validation of any neural coding model is required. This is done by contrasting its performance
933 against real behavioral sensory results for the animals under study [26]. Additionally, without the
934 precise quantification of the animal performance for a particular behavioral task, responding to natural
935 stimulus, it will not be possible to access the extended validity of any proposed model. Thus, both the
936 animal capacity and the theoretical model need to be contrasted.

937 Clearly, those constraints constitute high level challenges for the scientific community. Probably, this
938 is only the beginning of a long story.

939 1.7 Online Resources

940 1.7.1 Database

941 [Webvision. The Organization of the Retina and Visual System](http://webvision.med.utah.edu/)

942 <http://webvision.med.utah.edu/>

943 This site summarizes recent advances in knowledge and understanding of the visual system through
944 dedicated chapters and evolving discussion to serve as a clearing house for all things related to retina and
945 vision science.

946 [The brain from top to bottom: the retina](http://thebrain.mcgill.ca/flash/d/d_02/d_02_cl/d_02_cl_vis/d_02_cl_vis.html)

947 http://thebrain.mcgill.ca/flash/d/d_02/d_02_cl/d_02_cl_vis/d_02_cl_vis.html

948 This web site contains a series of topics dealing with the brain: "memory and the brain", "evolution and
949 the brain" and so on. Each topic is developed at different levels: beginner, intermediate, advanced. This
950 is a very useful and didactic reference.

951 [Information Processing in the Retina](http://www.sumanasinc.com/webcontent/animations/content/receptivefields.html)

952 <http://www.sumanasinc.com/webcontent/animations/content/receptivefields.html>

953 This page contains an animation illustrating the functioning of On-Off Receptive Fields. This is part of the
954 web site <http://www.sumanasinc.com/webcontent/animations.html> which contains nice animations
955 on different topics, including neuroscience.

956 [Multi Electrode arrays](http://en.wikipedia.org/wiki/Multielectrode_array)

957 http://en.wikipedia.org/wiki/Multielectrode_array

958 From the famous web site wikipedia.

960 [Paul Avery's Home Page. Image Gallery: Vision and the Eye](http://www.phys.ufl.edu/~avery/course/3400/gallery/gallery_vision.html)

961 http://www.phys.ufl.edu/~avery/course/3400/gallery/gallery_vision.html

962 This page contains a series of nice pictures illustrating the functioning of eyes and vision.

1.7.2 Software

[Event neural assembly Simulation](#)

<http://enas.gforge.inria.fr/v2/>

EnaS is a library providing numerical tools for the mesoscopic simulation of neural networks (temporal computations in micro-columns models or spiking neural networks) and the analysis of spike trains either coming from neural simulators or from biological experiments.

[Virtual Retina](#)

<http://www-sop.inria.fr/neuromathcomp/public/software/virtualretina/>

Virtual Retina is a simulation software developed at INRIA Sophia Antipolis - Méditerranée by Adrien Wohrer during his PhD (2005-2008) supervised by Pierre Kornprobst and Thierry Viéville.

Virtual Retina allows large-scale simulations of biologically-plausible retinas, with customizable parameters, and different possible biological features

Acknowledgment

This work has been supported by ERC grant Nervi 227747 (BC), European grant BrainScales (BC), ANR-CONICYT grant (KEOPS), FONDECYT 1110292 (AP) and ICM-IC09-022-P (AP).

List of Acronyms

P Photoreceptor
 B cell Bipolar Cell
 H cell Horizontal Cell
 A cell Amacrine Cell
 RF Receptive Field
 IF Integrate and Fire

References

1. *Principles of Neural Science. 4th edition.* McGraw-Hill, 2000.
2. S.-I. Amari. Information geometry of multiple spike trains. In Sonja Grün and Stefan Rotter, editors, *Analysis of Parallel Spike trains*, volume 7 of *Springer Series in Computational Neuroscience*, part 11, pages 221–253. Springer, 2010. DOI: 10.1007/978-1-4419-5675.
3. J.J. Atick. Could information theory provide an ecological theory of sensory processing? *Network: Computation in Neural Systems*, 3(2):213–251, 1992.
4. B.B. Averbeck, P.E. Latham, and A. Pouget. Neural correlations, population coding and computation. *Nat Rev Neurosci*, 7(5):358–66, 2006.
5. V. Balasubramanian and P. Sterling. Receptive fields and functional architecture in the retina. *J Physiol (Lond)*, 587(12):2753–67, 2009.
6. I.H. Brivanlou, D.K. Warland, and M. Meister. Mechanisms of concerted firing among retinal ganglion cells. *Neuron*, 20(3):527–39, 1998.
7. B. Cessac. Statistics of spike trains in conductance-based neural networks: Rigorous results. *Journal of Computational Neuroscience*, 1(8), 2011.
8. B. Cessac, H. Paugam-Moisy, and T. Viéville. Overview of facts and issues about neural coding by spikes. *J. Physiol. Paris*, 104(1-2):5–18, February 2010.
9. B. Cessac and T. Viéville. On dynamics of integrate-and-fire neural networks with adaptive conductances. *Frontiers in neuroscience*, 2(2), July 2008.
10. J.R. Chazottes and G. Keller. *Pressure and Equilibrium States in Ergodic Theory*, chapter Ergodic Theory. Encyclopedia of Complexity and System Science, Springer, 2009.
11. S. Cocco, S. Leibler, and R. Monasson. Neuronal couplings between retinal ganglion cells inferred by efficient inverse statistical physics methods. *PNAS*, 106(33):14058–14062, 2009.
12. I.P. Cornfeld, S.V. Fomin, and Y.G. Sinai. *Ergodic Theory*. Springer, Berlin, Heidelberg, New York, 1982.
13. J.B. Demb, K. Zaghloul, and P. Sterling. Cellular basis for the response to second-order motion cues in y retinal ganglion cells. *Neuron*, 32:711721, 2001.
14. S.H. DeVries. Correlated firing in rabbit retinal ganglion cells. *Journal of Neurophysiology*, 81(2):908–920, 1999.

- 1012 15. J.E. Dowling. *The retina: an approachable part of the brain*. Harvard University Press, Cambridge, Mass. (USA).,
1013 1987.
- 1014 16. R. Fernandez and G. Maillard. Chains with complete connections : General theory, uniqueness, loss of memory and
1015 mixing properties. *J. Stat. Phys.*, 118(3-4):555–588, 2005.
- 1016 17. G.D. Field and E.J. Chichilnisky. Information processing in the primate retina: circuitry and coding. *Annu Rev*
1017 *Neurosci*, 30:1–30, 2007.
- 1018 18. E. Ganmor, R. Segev, and E. Schneidman. The architecture of functional interaction networks in the retina. *The*
1019 *journal of neuroscience*, 31(8):3044–3054, 2011.
- 1020 19. E. Ganmor, R. Segev, and E. Schneidman. Sparse low-order interaction network underlies a highly correlated and
1021 learnable neural population code. *PNAS*, 108(23):96799684, 2011.
- 1022 20. W.S. Geisler. Visual perception and the statistical properties of natural scenes. *Annu. Rev. Psychol.*, 59:167–192, 2008.
- 1023 21. W.S. Geisler, J.S. Perry, and A.D. Ing. Natural systems analysis. *Human Vision and Electronic Imaging XIII*,
1024 6806:8060–M8060, 2008.
- 1025 22. H.-O. Georgii. *Gibbs measures and phase transitions*. De Gruyter Studies in Mathematics:9. Berlin; New York, 1988.
- 1026 23. I.I. Gikhman and A.V. Skorokhod. *The Theory of Stochastic Processes*. Springer, 1979.
- 1027 24. T. Gollisch and M. Meister. Eye smarter than scientists believed: neural computations in circuits of the retina. *Neuron*,
1028 65(2):150–164, January 2010.
- 1029 25. J. M. Hammersley and P. Clifford. Markov fields on finite graphs and lattices. *unpublished*, 1971.
- 1030 26. A.L. Jacobs, G. Fridman, R.M. Douglas, N.M. Alam, P.E. Latham, G.T. Prusky, and S. Nirenberg. Ruling out and
1031 ruling in neural codes. *Proc Natl Acad Sci U S A*, 106(14):5936–41, 2009.
- 1032 27. E.T. Jaynes. Information theory and statistical mechanics. *Phys. Rev.*, 106:620, 1957.
- 1033 28. G. Keller. *Equilibrium States in Ergodic Theory*. Cambridge University Press, 1998.
- 1034 29. K. Koch, J. McLean, M. Berry II, P. Sterling, V. Balasubramanian, and M.A. Freed. Efficiency of information trans-
1035 mission by retinal ganglion cells. *Curr Biol*, 14(17):1523–30, 2004.
- 1036 30. K. Koch, J. McLean, R. Segev, M.A. Freed, M.J. Berry II, V. Balasubramanian, and P. Sterling. How much the eye
1037 tells the brain. *Curr Biol*, 16(14):1428–34, 2006.
- 1038 31. B.G. Lindsey, K.F. Morris, R. Shannon, and G.L. Gerstein. Repeated patterns of distributed synchrony in neuronal
1039 assemblies. *Journal of Neurophysiology*, 78:1714–1719, 1997.
- 1040 32. N.K Logothetis. Vision: A window on consciousness. *Scientific American*, 281:44–51, 1999.
- 1041 33. G. Maillard. *Introduction to chains with complete connections*. Ecole Federale Polytechnique de Lausanne, winter 2007.
- 1042 34. O. Marre, S. El Boustani, Y. Frégnac, and A. Destexhe. Prediction of spatiotemporal patterns of neural activity from
1043 pairwise correlations. *Phys. rev. Let.*, 102:138101, 2009.
- 1044 35. L. Martignon, G. Deco, K. Laskey, M. Diamond, W. Freiwald, and E. Vaadia. Neural coding: Higher-order temporal
1045 patterns in the neurostatistics of cell assemblies. *Neural Computation*, 12(11):2621–2653, November 2000.
- 1046 36. L. Martignon, H. von Hasseln, S. Grün, A. Aertsen, and G. Palm. Detecting higher-order interactions among the spiking
1047 events in a group of neurons. *Biological Cybernetics*, 73(1):69–81, July 1995.
- 1048 37. R. Masland. The fundamental plan of the retina. *Nature neuroscience*, 4(9), September 2001.
- 1049 38. R.H. Masland and P.R. Martin. The unsolved mystery of vision. *Curr Biol*, 17(15):R577–82, 2007.
- 1050 39. D.N. Mastronarde. Correlated firing of cat retinal ganglion cells. I. Spontaneously active inputs to X-and Y-cells.
1051 *Journal of Neurophysiology*, 49(2):303–324, 1983.
- 1052 40. M. Meister, J. Pine, and D.A. Baylor. Multi-neuronal signals from the retina: acquisition and analysis. *J Neurosci*
1053 *Methods*, 51(1):95–106, 1994.
- 1054 41. S. Nirenberg, S. M. Carcieri, A. L. Jacobs, and P. E. Latham. Retinal ganglion cells act largely as independent encoders.
1055 *Nature*, 411(6838):698–701, 2001.
- 1056 42. I.E. Ohiorhenuan, F. Mechler, K.P. Purpura, A.M. Schmid, Q. Hu, and J.D. Victor. Sparse coding and high-order
1057 correlations in fine-scale cortical networks. *Nature*, 466(7):617–621, 2010.
- 1058 43. B.A. Olshausen and D.J. Field. Natural image statistics and efficient coding. *Network*, 7(2):333–9, 1996.
- 1059 44. S. Panzeri and S.R. Schultz. A unified approach to the study of temporal, correlational, and rate coding. *Neural*
1060 *Comput*, 13:1311–1349, 2001.
- 1061 45. A. Petrusca, D. Grivich, M. Sher, A. Field, G. Gauthier, J. Greschner, M. Shlens, J. Chichilnisky, and E. Litke.
1062 Identification and characterization of a y-like primate retinal ganglion cell type. *J Neurosci*, 27(41):11019–27, 2007.
- 1063 46. J.W. Pillow, L. Paninski, V.J. Uzzell, E.P. Simoncelli, and E.J. Chichilnisky. Prediction and decoding of retinal ganglion
1064 cell responses with a probabilistic spiking model. *J. Neurosci*, 25:11003–11013, 2005.
- 1065 47. A. Pouget, P. Dayan, and R. Zemel. Information processing with population codes. *Nat Rev Neurosci*, 1(2):125–32,
1066 2000.
- 1067 48. F. Rieke, D. Warland, R. de Ruyter van Steveninck, and W. Bialek. *Spikes: Exploring the Neural Code*. Bradford
1068 Books, 1997.
- 1069 49. R. L. Rockhill, F. J. Daly, M. A. MacNeil, S. P. Brown, and R. H. Masland. The diversity of ganglion cells in a
1070 mammalian retina. *J Neurosci*, 22(9):3831–43, 2002.
- 1071 50. R. W. Rodieck. Maintained activity of cat retinal ganglion cells. *J Neurophysiol*, 30(5):1043–71, 1967.
- 1072 51. Y. Roudi, E. Aurell, and J.A. Hertz. Statistical physics of pairwise probability models. *Frontiers in Computational*
1073 *Neuroscience*, page 15, 2009.
- 1074 52. Y. Roudi and J. Hertz. Mean field theory for non-equilibrium network reconstruction. *Phys. Rev. Lett.*, 106(048702),
1075 2011.
- 1076 53. Y. Roudi and J.A. Hertz. Mean field theory for non-equilibrium network reconstruction. *arXiv*, page 11, Sept 2010.
- 1077 54. Y. Roudi, S. Nirenberg, and P.E. Latham. Pairwise maximum entropy models for studying large biological systems:
1078 when they can work and when they can't. *PLOS Computational Biology*, 5(5), 2009.
- 1079 55. Y. Roudi, J. Tyrcha, and J.A. Hertz. Ising model for neural data: Model quality and approximate methods for extracting
1080 functional connectivity. *Physical Review E*, page 051915, 2009.

- 1081 56. M. Rudolph and A. Destexhe. Analytical integrate and fire neuron models with conductance-based dynamics for event
1082 driven simulation strategies. *Neural Computation*, 18:2146–2210, 2006.
- 1083 57. D. Ruelle. *Thermodynamic formalism*. Addison-Wesley, Reading, Massachusetts, 1978.
- 1084 58. R. Sarpeshkar. *Ultra Low Power Bioelectronics: Fundamentals, Biomedical Applications, and Bio-Inspired Systems*.
1085 Cambridge University Press, 2010.
- 1086 59. M.T. Schaub and S.R. Schultz. The ising decoder: reading out the activity of large neural ensembles. *arXiv:1009.1828*,
1087 2010.
- 1088 60. E. Schneidman, M.J. Berry II, R. Segev, and W. Bialek. Weak pairwise correlations imply strongly correlated network
1089 states in a neural population. *Nature*, 440(7087):1007–1012, 2006.
- 1090 61. E. Schneidman, W. Bialek, and M.J. Berry II. Synergy, redundancy, and independence in population codes. *J Neurosci*,
1091 23(37):11539–53, 2003.
- 1092 62. G. Schwartz and M.J. Berry II. Sophisticated temporal pattern recognition in retinal ganglion cells. *J Neurophysiol*,
1093 99(4):1787–98, 2008.
- 1094 63. R. Segev, I. Baruchi, E. Hulata, and E. Ben-Jacob. Hidden neuronal correlations in cultured networks. *Physical Review*
1095 *Letters*, 92:118102, 2004.
- 1096 64. E. Seneta. *Non-negative Matrices and Markov Chains*. Springer, 2006.
- 1097 65. J. Shlens, G.D. Field, J. L. Gauthier, M.I. Grivich, D. Petrusca, A. Sher, A. M. Litke, and E.J. Chichilnisky. The
1098 structure of multi-neuron firing patterns in primate retina. *J Neurosci*, 26(32):8254–66, 2006.
- 1099 66. J. Shlens, G.D. Field, J.L. Gauthier, M. Greschner, A. Sher, A.M. Litke, and E.J. Chichilnisky. The structure of
1100 large-scale synchronized firing in primate retina. *The Journal of Neuroscience*, 29(15):5022–5031, April 2009.
- 1101 67. E.P. Simoncelli and B.A. Olshausen. Natural image statistics and neural representation. *Annu Rev Neurosci*, 24:1193–
1102 216, 2001.
- 1103 68. S.P. Strong, R. Koberle, R.R. de Ruyter van Steveninck, and W. Bialek. Entropy and information in neural spike trains.
1104 *Phys. Rev. Lett*, 80(1):197–200, 1998.
- 1105 69. M. Taketani and M. Baudry. *Advances in Network Electrophysiology: Using Multi-Electrode Arrays*. Springer, 2006.
- 1106 70. E. Thompson, A. Palacios, and F. Varela. Ways of coloring: Comparative color vision as case study for cognitive science.
1107 *Behavioral and Brain Sciences*, 15:1–75, 1992.
- 1108 71. G. Tkačik, E. Schneidman, M.J. Berry II, and W. Bialek. Spin glass models for a network of real neurons. *arXiv*,
1109 page 15, 2009.
- 1110 72. J. L. Van Hemmen and T.J. Sejnowski. 23 problems in systems neuroscience. *Oxford University Press, Inc.*, 2006.
- 1111 73. J.-C. Vasquez, H. Nasser, A. Palacios, B. Cessac, T. Viéville, and H. Rostro-Gonzalez. Parametric estimation of
1112 spike train statistics by gibbs distributions : an application to bio-inspired and experimental data. In *Proceedings of*
1113 *Neurocomp 2010 (Lyon)*, 2010.
- 1114 74. J.-C. Vasquez, A.G. Palacios, O. Marre, M.J. Berry II, and B. Cessac. Gibbs distribution analysis of temporal correlation
1115 structure on multicell spike trains from retina ganglion cells. *J. Physiol. Paris*, 2011. submitted.
- 1116 75. J.-C. Vasquez, T. Viéville, and B. Cessac. Entropy-based parametric estimation of spike train statistics. *Journal of*
1117 *Computational Neuroscience*, 2010. submitted.
- 1118 76. A.E.P. Villa, I.V. Tetko, B. Hyland, and A. Najem. Spatiotemporal activity patterns of rat cortical neurons predict
1119 responses in a conditioned task. *Proc Natl Acad Sci USA*, 96(3):1106–1111, 1999.
- 1120 77. A. Wöhrer and P. Kornprobst. Virtual retina: a biological retina model and simulator, with contrast gain control.
1121 *Journal of Computational Neuroscience*, 26(2):219–249, 2009.

1122 References

Index

- 1124 Biophysics
 - 1125 amacrine cells, viii
 - 1126 bipolar cells, viii
 - 1127 functional connectivity, xxv
 - 1128 horizontal cells, viii
 - 1129 photoreceptors, viii
 - 1130 raster plot, xi
 - 1131 receptive field, ix
- 1132 Mathematics
 - 1133 Bernoulli model, xxi
 - 1134 empirical average, xvii
 - 1135 Gibbs distribution, xv
 - 1136 Gibbs potential, xv
 - 1137 Ising potential, xxi
 - 1138 Kullback-Leibler divergence (KL), xxiii
 - 1139 memory depth, xiii
 - 1140 monomials, xvi
 - 1141 observable, xvi
 - 1142 raster plot, xiii
 - 1143 spiking pattern, xiii
 - 1144 stationarity, xv, xvii
 - 1145 time average, xvii